frontiers | Frontiers in Marine Science

TYPE Original Research
PUBLISHED 14 February 2024
DOI 10.3389/fmars.2024.1304118

OPEN ACCESS

EDITED BY
Antonio Cobelo-Garcia,
Spanish National Research Council (CSIC), Spain

REVIEWED BY
Aridane G. Gonzalez,
University of Las Palmas de Gran Canaria, Spain
Laramie Jensen,
University of Washington, United States

*CORRESPONDENCE
Léo Mahieu
leo.mahieu@oregonstate.edu;
leo.mahieu@live.fr

RECEIVED 28 September 2023
ACCEPTED 08 January 2024
PUBLISHED 14 February 2024

CITATION
Mahieu L, Whitby H, Dulaquais G, Tilliette C, Guigue C, Tedetti M, Lefevre D, Fourrier P, Bressac M, Sarthou G, Bonnet S, Guieu C and Salaün P (2024) Iron-binding by dissolved organic matter in the Western Tropical South Pacific Ocean (GEOTRACES TONGA cruise GPpr14).
Front. Mar. Sci. 11:1304118.
doi: 10.3389/fmars.2024.1304118

Iron-binding by dissolved organic matter in the Western Tropical South Pacific Ocean (GEOTRACES TONGA cruise GPpr14)

Léo Mahieu[1,2]*, Hannah Whitby[1], Gabriel Dulaquais[3], Chloé Tilliette[4,5], Catherine Guigue[6], Marc Tedetti[6], Dominique Lefevre[6], Pierre Fourrier[7,8], Matthieu Bressac[5], Géraldine Sarthou[3], Sophie Bonnet[6], Cécile Guieu[5] and Pascal Salaün[1]

[1]School of Environmental Sciences, University of Liverpool, Liverpool, United Kingdom, [2]College of Earth, Ocean and Atmospheric Sciences, Oregon State University, Corvallis, OR, United States, [3]CNRS, Univ Brest, IRD, Ifremer, LEMAR, Plouzané, France, [4]CNRS, Univ. Littoral Côte d'Opale, UMR 8187 – LOG – Laboratoire d'Océanologie et de Géosciences, Univ. Lille, Lille, France, [5]Laboratoire d'Océanographie de Villefranche, CNRS UMR7093, Sorbonne Université, Villefranche-sur-Mer, France, [6]Aix-Marseille Univ., Universiteé de Toulon, CNRS, IRD, MIO UM 110, Marseille, France, [7]Conservatoire National des Arts et Métiers INTECHMER, Cherbourg, France, [8]Laboratoire des Sciences Appliquées de Cherbourg, Normandie University, UNICAEN, Cherbourg, France

Iron (Fe) is an essential micronutrient for phytoplankton growth, but its scarcity in seawater limits primary productivity across much of the ocean. Most dissolved Fe (DFe) in seawater is complexed with Fe-binding organic ligands, a poorly constrained fraction of dissolved organic matter (DOM), which increase Fe residence time and impact Fe bioavailability. Here, we present the conditional concentration (L_{Fe}) and binding-strength (log $K^{cond}_{Fe'L}$) of Fe-binding ligands in the Western Tropical South Pacific (WTSP) Ocean during the GEOTRACES TONGA cruise (GPpr14). The transect crossed the Lau basin, a region subject to shallow hydrothermal Fe inputs that fuel intense diazotrophic activity, the oligotrophic South Pacific gyre, and the Melanesian basin. Organic speciation was analyzed by competitive ligand exchange adsorptive cathodic stripping voltammetry (CLE-AdCSV) using salicylaldoxime at 25 µM. We found a high mean L_{Fe} of 5.2 ± 1.2 nMeqFe (n = 103) across the entire transect, predominantly consisting of intermediate strength L2 ligands (84%; mean log $K^{cond}_{Fe'L}$ of 11.6 ± 0.4), consistent with humic-like substances. DFe correlated with the humic-like component of the fluorescent DOM (HS-like FDOM), yet the electroactive Fe-binding humic-like substances (L_{FeHS}) accounted for only 20 ± 13% of L_{Fe} in the mixed layer and 8 ± 6% in deep waters. Ligands were in large excess compared to DFe (mean excess ligand eL_{Fe} = 4.6 ± 1.1 nMeqFe), suggesting poor stabilization of DFe inputs. High L_{Fe} (up to 9 nMeqFe) in samples close to hydrothermal sites could be due to detoxification strategies from plankton communities toward hydrothermally-fueled toxic trace metals other than Fe, with an apparent dilution of the DOM from the Lau basin into neighboring regions. We also observed a different peak potential of the Fe salicylaldoxime complex detected by CLE-AdCSV between the Lau and Melanesian basins, and between surface and deep waters. To our knowledge, this change in potential has not previously been

reported; whether this represents a novel detection of specificities in DOM composition merits further investigation. Competition between Fe and competing metals for ligand binding sites could favor DFe oxidation and precipitation near hydrothermal vents and explain the absence of strong Fe stabilization in the WTSP.

KEYWORDS

iron-binding ligands, hydrothermal, diazotroph, remineralization, humic substances, voltammetry, fluorescence

Introduction

Iron (Fe) is an essential micronutrient for phytoplankton growth because of its role in multiple metabolic processes (Twining and Baines, 2013). Biological Fe demand is such that its availability co-limits primary production across around 40% of the ocean (Moore et al., 2013; Browning and Moore, 2023). Fe scarcity is also explained by its very low solubility in seawater (Liu and Millero, 2002). Fe is quickly hydrolyzed and exported as oxyhydroxide aggregates in oxygenated conditions (Liu and Millero, 2002), and as Fe-sulfide (e.g., pyrite) in more anoxic environments such as hydrothermal vents (Rickard and Luther, 2007). However, despite its low solubility and inorganic scavenging, the Fe concentration found in the dissolved fraction (DFe; defined by the filter of 0.2 µm or 0.45 µm pore size) is higher than what is expected from its inorganic speciation (Liu and Millero, 2002). This is partly explained by extensive complexation of DFe by a fraction of the dissolved organic matter (DOM) pool, known as Fe-binding ligands, that enhance Fe solubility and increase its residence time in surface waters, thereby impacting its bioavailability to phytoplankton. It is generally accepted that most DFe (> 99%) is complexed to organic ligands (Gledhill and Buck, 2012). Knowledge of the nature and cycling of these ligands is required to understand and predict Fe distribution and bioavailability in seawater, but obtaining this information is challenging. Characterization of the Fe complexing fraction is difficult because of the sheer chemical diversity of DOM (Mentges et al., 2017; Dittmar et al., 2021) and the relatively low abundance of Fe-binding compounds, only exceeding DFe by around 1 nmol equivalent of Fe per liter (nMeqFe) in the global ocean (Gledhill and Buck, 2012; Boyd and Tagliabue, 2015). Various methods enable measurements of the major individual Fe-binding ligand groups, namely siderophores (Bundy et al., 2018; Boiteau and Repeta, 2022), humic-like substances (HS-like; Laglera and van den Berg, 2009; Pernet-Coudrier et al., 2013; Whitby and van den Berg, 2015; Sukekava et al., 2018), and exopolymeric substances (EPS; Hassler et al., 2011; Hassler et al., 2015; Norman et al., 2015). Those methods, however, have a limited resolution because of the diversity encountered within each group.

The challenge of identifying individual ligands within the range of metal-binding compounds composing DOM is overcome by Competitive Ligand Exchange (CLE). This approach is based on the competition between the natural Fe-binding ligands and an added competitive ligand at increasing DFe concentrations. The titration of the natural Fe-binding ligands is monitored by adsorptive cathodic stripping voltammetry (AdCSV), quantifying the electrons needed to reduce the DFe that formed an electroactive complex with the added ligand. This approach allows the determination of the maximum amount of DFe that can be complexed by the natural DOM present within a sample, defined as the Fe-binding ligand concentration (L_{Fe}), and the averaged conditional stability constant (log $K^{cond}_{Fe'L}$) of the Fe-binding complexes within the detection window ($\alpha_{Fe'AL}$) applied. The detection window is defined as the product of the added ligand concentration ([AL]) forming the electroactive complex $FeAL_n$ and of its binding affinity with DFe ($\beta^{cond}_{Fe'AL}$; $\alpha_{Fe'AL} = [AL]^n * \beta^{cond}_{Fe'AL}$). The log $K^{cond}_{Fe'L}$ values obtained by CLE-AdCSV are commonly divided into classes, with L_1 corresponding to strong Fe-binding ligands (log $K^{cond}_{Fe'L}$ > 12), L_2 to intermediate ligands (10< log $K^{cond}_{Fe'L}$ < 12) and L_3 to weak ligands (log $K^{cond}_{Fe'L}$ < 10; Gledhill and Buck, 2012). These classes roughly correspond to the three major types of ligands identified in the environment, with siderophores falling into the L_1 class, HS into L_2, and EPS into L_3 (Hassler et al., 2017), although classes can overlap and remain a simplistic view of the Fe organic speciation. For example, accumulating evidence suggests HS encompass multiple binding sites across the L_1 and L_2 ligand classes and are able to compete with siderophores (Fourrier et al., 2022; Gledhill et al., 2022; Sukekava et al., 2024). The log $K^{cond}_{Fe'L}$ of specific functional groups has also been determined and their contribution to the pool of Fe-binding ligands highlighted (e.g., Santana-Casiano et al., 2000; González et al., 2019). However, in natural samples, the binding ability of the DOM is a continuum of log $K^{cond}_{Fe'L}$ values rather than a specific value as determined by CLE-AdCSV (Town and Filella, 2000). Indeed, the log $K^{cond}_{Fe'L}$ determined by CLE-AdCSV is an average value of all the titrated ligands, and it is not well understood how the log $K^{cond}_{Fe'L}$ of each compound or functional group is weighted during the titration of a continuum of ligands. In all, while being mindful of limitations, this classification remains a helpful way to interpret and compare Fe-binding ligand data.

Fe-binding ligand distribution is often characterized by high L_{Fe} and $K^{cond}_{Fe'L}$ surface waters with maximum values coinciding with the chlorophyll-a maximum, and progressive decrease from the surface

until the oxycline due to adsorption onto particles (Kondo et al., 2007: Ibisanmi et al., 2011; Gledhill and Buck, 2012; Gerringa et al., 2015; Bundy et al., 2016). Phytoplankton production of L_{Fe} has been widely attested by concomitant L_{Fe} and chlorophyll-a fluorescence (Gledhill and Buck, 2012; Gerringa et al., 2015; Bundy et al., 2016; Hassler et al., 2017). L_{Fe} depletion can sometimes be observed in surface waters due to photochemical breakdown of ligands, but this process is highly variable (Barbeau et al., 2001; Powell and Wilson-Finelli, 2003; Croot et al., 2004), while atmospheric deposition such as dust and rain supply Fe-binding ligands to surface waters (Gerringa et al., 2006; Rijkenberg et al., 2008; Cheize et al., 2012; González et al., 2022). Below the oxycline, L_{Fe} increases through the breakdown of biogenic material by heterotrophic bacteria (Boyd et al., 2010) which produce Fe-binding ligands that are mostly attributed to HS due to their intermediate log $K^{cond}_{Fe'L}$ and relatively homogenous distribution in deep waters (van den Berg, 1995; Witter and Luther, 1998; van den Berg, 2006; Dulaquais et al., 2018; Whitby et al., 2020b). Heterotrophic bacteria produce siderophore compounds, associated with the breakdown of sinking particles (Cordero et al., 2012; Bundy et al., 2016; Velasquez et al., 2016; Hassler et al., 2017) while the resuspension of sediments and hydrothermal activity are important sources of Fe-binding ligands to bottom waters (Jones et al., 2011; Gerringa et al., 2015; Tagliabue and Resing, 2016. Buck et al., 2018; Sukekava et al., 2023).

The classification of binding strength presented by Gledhill and Buck (2012) has been used to compare basin scale datasets of Fe-binding ligand characteristics from samples collected in the West and North Atlantic Oceans (Buck et al., 2015; Gerringa et al., 2015), and in the Tropical Pacific Ocean (Buck et al., 2018). In addition to a general trend of decreasing log $K^{cond}_{Fe'L}$ and increasing L_{Fe} with depth and water mass aging, L_1 has been shown to correlate with increasing DFe concentrations around hydrothermal vents in the Atlantic and Pacific Oceans (Buck et al., 2015; Buck et al., 2018) and with vent communities supplying siderophores specifically (Hoffman et al., 2023). L_1 ligands were also observed in hydrothermal fluid samples collected at the New Hebrides Island arc in the Western Tropical South Pacific (WTSP) Ocean with concentrations reaching the micromolar range for L_{Fe} and DFe (Kleint et al., 2016). These authors also detected weaker L_3 ligands in several WTSP Ocean hydrothermal samples, while intermediate L_2 ligands have been observed in hydrothermal plumes in the Mariana Back Arc of the Western Pacific (Wang et al., 2021) and in the Southern Ocean (Hawkes et al., 2013).

In hydrothermal fluids, concentrations of DFe and Fe-binding ligands can vary from the nM to µM range depending on the initial fluid chemistry (e.g., Hawkes et al., 2013; Resing et al., 2015; Kleint et al., 2016; Tilliette et al., 2022). The chemistry of hydrothermal fluids is geographically diverse and variable over time, and sampling in such dynamic environments is challenging, making hydrothermal Fe-binding ligand chemistry complicated to constrain (Kleint et al., 2019). In terms of DFe, it is well known that the free ionic Fe^{2+} initially found in hot and acidic hydrothermal fluid is quickly oxidized and precipitated during mixing with seawater by the formation of Fe-sulfides and Fe-oxyhydroxide minerals (Millero et al., 1987; Kleint et al., 2017), but it can also be adsorbed on organic matrices or stabilized by Fe-binding ligands (Toner et al., 2009; Sander and Koschinsky, 2011; Kleint et al., 2017; Santana-Casiano et al., 2022). The inorganic transport of DFe as Fe-sulfide nanoparticles and colloidal Fe-oxyhydroxides has also been observed and the accessibility of these fractions to Fe-binding ligands is controversial (Yücel et al., 2011; Yücel et al., 2021). Recent work showed that electroactive humic component of Fe-binding ligands (L_{FeHS}) can solubilize a large fraction of freshly formed Fe-oxyhydroxides, but this decreases rapidly with aging of the inorganic particles. This experiment was performed at constant temperature and pH (Dulaquais et al., 2023) but is yet to be addressed under variable physicochemical conditions such as during the dilution of hydrothermal plumes. The variable interplay between the inorganic and organic processes impacting the amount of DFe stabilized and transported away from hydrothermal sources is an essential aspect to constrain, as vents could account for an estimated 12-22% of the deep-ocean DFe budget (Bennett et al., 2008).

In the WTSP Ocean, the subduction of the Pacific Plate beneath the Australian Plate has formed the Tonga volcanic arc, one of the most seismically active subduction zones which consequently hosts a high density of submarine volcanoes and associated hydrothermal vents (German et al., 2006; Timm et al., 2013). The submarine hydrothermal activity fuels the area with DFe (Guieu et al., 2018; Tilliette et al., 2022), supporting the growth of nitrogen fixers (diazotroph). Some of the highest rates of dinitrogen (N_2) fixation ever observed in open ocean have been measured in the area (Bonnet et al., 2017; Bonnet et al., 2018), specifically in the Lau basin, but the mechanistic link between shallow hydrothermal Fe inputs and intense N_2 fixation has only been recently demonstrated (Bonnet et al., 2023b). The possibility to investigate the connection between hydrothermal sourcing of trace metals and the fueling of diazotroph activity motivated the GEOTRACES process cruise GPpr14 (TONGA cruise; Guieu and Bonnet, 2019, https://doi.org/10.17600/18000884), which crossed the Melanesian basin, the Lau basin, and the western part of the South Pacific gyre between October 31st and December 5th, 2019.

The TONGA transect presented the opportunity to quantify, for the first time in this region, L_{Fe} and log $K^{cond}_{Fe'L}$, and to explore the relation between Fe-binding ligands and DFe distribution in the area. Several complementary analyses targeting specific fractions of the DOM pool were also conducted, notably regarding HS-like material. HS are of specific interest as they have been estimated to represent around 50% of the DOM (Zigah et al., 2017; Fourrier et al., 2022) with a smaller fraction, around 5% of DOC, able to bind with Fe (Laglera and van den Berg, 2009; Fourrier et al., 2022). The diversity of the HS-like material is responsible for various properties, notably in terms of electroactivity and photo-reactivity, the latter in terms of absorbance and fluorescence (CDOM and FDOM, respectively). It has been shown that electroactive Fe-HS complexes (L_{FeHS}) are able to control Fe solubility in a variety of systems (Dulaquais et al., 2018; Sukekava et al., 2018; Laglera et al., 2019; Whitby et al., 2020b; Fourrier et al., 2022). Similarly, the HS-like fluorescent component of the DOM (HS-like FDOM) often correlates with DFe distributions (Tani et al., 2003; Ohno et al., 2008; Hioki et al., 2014; Jia et al., 2021).

The complementarity and/or overlapping of these two different operationally defined fractions of HS is, however, not well constrained. While covariation of L_{FeHS} and HS-like FDOM is observed in estuarine waters (Lee et al., 2023), opposite trends are observed in open ocean surface waters, suggesting that the microbial aerobic respiration of the DOM increases the fluorescent yields and lowers the electroactivity of the HS fraction of the DOM with depth (Fourrier et al., 2022).

We present here the results obtained for Fe-binding ligand characteristics during the TONGA cruise using the same competitive ligand method that was used in both the Equatorial Pacific (Buck et al., 2018) and the North Atlantic Oceans (Buck et al., 2015). We relate the distribution observed in L_{Fe} and log $K^{cond}_{Fe'L}$ to other parameters such as DFe, apparent oxygen utilization (AOU), dissolved organic carbon (DOC), L_{FeHS} and HS-like FDOM to identify the processes impacting Fe-binding ligands and HS-like compounds, and to constrain their impact on DFe distribution in the WTSP Ocean.

Material and methods

Sampling strategy during the TONGA cruise

Samples were collected during the TONGA GEOTRACES process study in the WTSP Ocean (GPpr14). The section presented here is composed of 8 main stations between the Melanesian basin and the South Pacific gyre (Figure 1), with additional casts performed around two known hydrothermal sites, LD 5 and LD 10, identified by acoustic detection (Bonnet et al., 2023b). Here, we present data for one of the hydrothermal stations, LD10, for which stations LD 10-T1, T2 and T3 were sampled at 15, 8, and 2 km from the hydrothermal source, respectively. The western part of the Lau basin was sampled at stations 4, 11 and 12. Stations 2 and 3 were located in the Melanesian basin, on the western side of the transect. Stations 6, 7 and 8 were located in the South Pacific gyre for comparison with oligotrophic conditions. Station 6 was located East of the Tonga arc, but on the western side of the Tonga trench, where the topography is expected to limit water exchange between the Lau basin and the South Pacific gyre (Talley et al., 2011).

Sample collection and storage

The seawater samples for DFe and Fe-binding ligand analyses were collected using GO-FLO bottles mounted on a Trace Metal Clean Rosette (TMR; General Oceanics Inc., Model 1,018 Intelligent Rosette) transferred into a trace metal clean van (class-100) and pressurized with 0.2 µm-filtered nitrogen (Air Liquide) for sub-sampling. GO-FLO bottles and all the sampling material were cleaned before the cruise following the GEOTRACES cookbook (Cutter et al., 2017). Dissolved fractions for the analysis of DFe and Fe-binding ligands were sampled through 0.45 µm acid-cleaned polyethersulfone filters (Supor). For DFe, the cleaning procedure of the bottles used for seawater collection, sample storage, handling and analyses are detailed in Tilliette et al. (2022).

For Fe-binding ligands, 250 mL low-density polyethylene (LDPE; Nalgene) bottles were left to soak for one week in a 2% surfactant bath (Decon), one week in a 1 M HCl bath (laboratory reagent grade 32%, FisherScientific) and one week in a 0.1 M HCl bath, before being left to dry in a laminar flow hood (Class-100) and double-bagged. Between each step, the bottles were rinsed 5-times with Milli-Q water (resistivity > 18.2 MΩ.cm). The samples were collected after rinsing the bottles 3 times with around 20 mL of filtered sample and frozen to -20°C immediately after sampling. Samples were thawed at room temperature in the dark and swirled before analysis.

The seawater samples for dissolved oxygen (O_2), DOC and FDOM analyses were collected in glass bottles from a classical rosette equipped with twenty-four 12 L Niskin bottles. The samples were immediately filtered under low vacuum (< 50 mm Hg) through pre-combusted 25-mm fiberglass filters (GF/F, size pore: ~0.7 µm, Whatman) using glass filtration apparatus. For DOC analyses, filtered samples were transferred into 10 mL glass ampoules and acidified with 20 µL of sulfuric acid (H_2SO_4, 95-98%, Sigma-Aldrich). Ampoules were then flame-sealed and stored in the dark at 4°C pending analysis. For FDOM measurements, filtered samples were

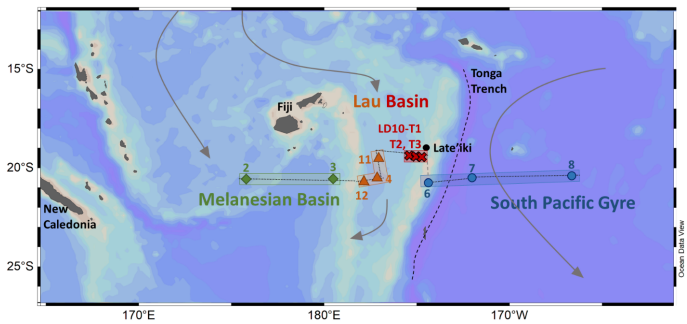

FIGURE 1
Map of the studied area, cruise transect and sampling stations for Fe-binding ligand characteristics during the TONGA cruise (GPpr14; Guieu and Bonnet, 2019, https://doi.org/10.17600/18000884). The small-dashed black line corresponds to the transect drawn to present the data. Colors, symbols and shapes correspond to the splitting of the dataset for presentation and interpretation. Geographic features (in black) include the main islands, the Tonga trench and the location of the Late'iki site.

transferred into 100 mL amber glass bottles with clean Teflon-lined caps and stored at -20°C in the dark before analysis. Before use, all glassware was left to soak for 24 h in a 1 M HCl bath, rinsed thoroughly with Milli-Q water, then combusted at 450°C for 6 h, and finally rinsed three times with the respective sample before filling.

Analyses

Detailed description of the analysis and interpretation for L_{FeHS}, CDOM/FDOM and DFe can be found in connected papers (Tilliette et al., 2022; Dulaquais et al., 2023; Tedetti et al., in prep.[1]). For L_{FeHS}, CDOM/FDOM, DFe, dissolved organic carbon and Fe-binding ligands, the seawater was filtered in-line using an acid-cleaned 0.45 µm polyethersulfone filter (Supor).

Dissolved oxygen

O_2 concentration was measured following the Winkler method (Winkler, 1888) modified by Carpenter (1965) and Carritt and Carpenter (1966), with potentiometric endpoint detection using a Titrino 716 DMS (Metrohm; Oudot et al., 1988). The recommendations from Langdon (2010) were followed for sampling, reagent preparation and analysis. The thiosulfate solution was calibrated by titrating it against a potassium iodate certified standard solution of 0.0100 N (CSK standard solution; WAKO). The reproducibility, expressed as the standard deviation of replicate samples, was 0.8 µM (n = 15, mean = 195.4 µmol kg^{-1}. Apparent Oxygen Utilization (AOU, in µM) was calculated from the difference between O_2 solubility concentration (at P = 0 dbar) estimated with the Benson and Krause coefficients (Garcia and Gordon, 1992) and *in-situ* O_2.

Dissolved organic carbon

DOC concentration was measured in two ampoule replicates on a Shimadzu TOC-V analyzer according to Sohrin and Sempéré (2005) and Fourrier et al. (2022). Before injection, the GF/F-filtered and acidified samples were bubbled for 2 min with CO_2-free air to purge inorganic carbon. The accuracy and system blank of the instrument were determined by the analysis of certified water references (batch 19, lot #03–19, Hansell Laboratory, Miami, USA). The nominal precision of the analysis procedure was within 2%.

Iron-binding ligands

The theory of the CLE-AdCSV approach has been thoroughly detailed in previous work (e.g., Gledhill and van den Berg, 1994; Rue and Bruland, 1995; Abualhaija and van den Berg, 2014; Gerringa et al., 2014; Pižeta et al., 2015; Mahieu, 2023). We used the added ligand salicylaldoxime (SA; 98% Acros Organics) at 25 µM following the procedure described in Mahieu (2023). For data interpretation the side reaction coefficient (β_{FeSA_2}) of 11.1 leading to $\alpha_{Fe'AL}$ of 79 was used, as in previous basin scale work (Buck et al., 2007; Buck et al., 2015; Buck et al., 2018). A borate buffer (boric acid, analytical reagent grade, Fisher Scientific) at 1 M in 0.35 M of ammonia (NH_4OH; 29% Laporte) was used at 10 mM for a final pH of 8.2 in the sample (Rue and Bruland, 1995; Buck et al., 2007; Abualhaija and van den Berg, 2014; Buck et al., 2015; Buck et al., 2018; Mahieu, 2023). The following equilibration procedure was applied: natural ligands were left to equilibrate with increasing additions of DFe in buffered samples for a minimum of 2 h, with SA added at least 15 min before the start of the analysis. The titrations were performed with 16 aliquots, with DFe additions of 0, 0, 0.75, 1.5, 2.25, 3, 3.5, 4, 4.5, 5, 6, 7, 8, 10, 12 and 15 nM. The DFe additions were adjusted from Buck et al. (2018) after preliminary tests showing emergence of the $FeSA_2$ reduction current around 3 nM of DFe added (nMeqFe). The sensitivity was estimated using the three last linear additions of the titration of the seawater sample. The apparatus and procedures for the conditioning of cells and tubes (Trace Metal Free, Labcon) are described in Mahieu (2023) and Mahieu et al. (2024), along with a detailed description of the set up and data treatment.

Statistical treatments

The variables considered in this study did not follow a normal distribution, and were inter-dependent and non-linear, calling for the application of non-parametric statistical methods. The significance of the difference between water masses and regions was tested using the Wilcoxon-Mann-Whitney test, using the Python function 'scipy.stats.mannwhitneyu'. The difference between two samples is defined by p values< 0.05. Full p value matrices can be found in Supplementary Information 2, 3. The Spearman rank correlation (ρ; Spearman, 1904) analysis was chosen to compare the Fe-binding characteristics and the other parameters described hereafter as it has been previously used for the investigation of Fe-binding ligands and FDOM (e.g., Heller et al., 2013; Genovese et al., 2018). The calculation was performed using the Python function 'scipy.stats.spearmanr' (version 3.9). For the Spearman test, ρ from 0.00 to 0.19 were attributed to very weak correlation, ρ from 0.20 to 0.39 to weak correlation, ρ from 0.40 to 0.59 to moderate correlation, ρ from 0.60 to 0.79 to strong correlation, and ρ from 0.80 to 0.99 to very strong correlation (ρ = 1.00 being a perfectly monotonic correlation). We considered the correlation to be significant for p< 0.0001, at least one order of magnitude lower than in other studies discussing Spearman correlation matrices including Fe-binding ligands data to ensure a strong level of confidence in the interpretation of the dataset (e.g., Heller et al., 2013; Genovese et al., 2018; bold values in Table 1).

Results

Hydrography

The water mass composition and circulation have been thoroughly described by Tilliette et al. (2022). We present here a simplistic description of the water column based on O_2 fluctuations (Figures 2, 3A). During the TONGA transect, surface waters were characterized by high O_2 due to primary production and

1 Tedetti, M., Guigue, C., Mahieu, L., Fourrier, P., Dulaquais, G., Benavides, M., et al. Chromophoric and fluorescent dissolved organic matter in the Western Tropical South Pacific.

TABLE 1 Mean values for DFe, L_{Fe}, L_{FeHS}, DOC and HS-like FDOM for the mixed layer and deep waters.

Considered data	DFe (nM)	L_{Fe}	L_{FeHS}		DOC (µgC L^{-1})	HS-like FDOM (QSU)
		(nMeqFe)	(nMeqFe)	(µgeqC L^{-1})		
Mixed layer	0.45 ± 0.50	5.3 ± 1.4	1.3 ± 0.7	40.2 ± 23.1	883 ± 53	1.7 ± 0.5
	n = 60	n = 24	n = 31		n = 40	n = 36
Deep waters	0.51 ± 0.30	5.2 ± 1.1	0.5 ± 0.3	12.5 ± 10.1	580 ± 126	2.5 ± 0.7
	n = 178	n = 79	n = 75		n = 129	n = 94

Estimates of Fe-binding equivalent concentrations for L_{FeHS} were calculated using 16.4 nmolFe.mgFA^{-1} from Sukekava et al. (2018). Estimates of carbon equivalent were calculated using the official value of 0.5244% gC/gSRFA (International Humic Substances Society).

atmospheric exchange enhanced by physical mixing in the mixed layer, which ranged from 70 to 140 m deep during the cruise. The water mass below the mixed layer corresponds to the Subtropical Underwater (STUW) in the South Pacific gyre and Lau basin, and to the Western South Pacific Central Water (WSPCW) in the Melanesian and Lau basins. Both STUW and WSPCW are characterized by a maximum of salinity (S) and minimum of O_2 around 200 m, the latter being due to microbial respiration (e.g., remineralization). Below these two water masses is the Antarctic Intermediate Water (AAIW), with a S minimum and an O_2 maximum (Figure 2) also corresponding to the thermocline at around 650 m depth (Kawabe and Fujio, 2010; Talley et al., 2011). Below the AAIW, S increases and temperature decreases. O_2 concentrations below 150 µmol kg^{-1} is characteristic of the Pacific Deep Water (PDW), originating from the upwelling of Antarctic Bottom Water (AABW) in the middle of the Pacific Ocean, mixing with the O_2 depleted waters from the Pacific oxygen minimum zone and with the deep waters from the oxygen minimum zone off Chile in the Eastern South Pacific Ocean (Silva et al., 2009). AAIW and PDW supposedly reach the Lau and Melanesian basins from a branch of the South Pacific gyre flowing from the North of the Lau basin following south-westward currents (Summers and Watling, 2021; Tilliette et al., 2022). However, the circulation in and between the Lau and Melanesian basins is variable, and northeast currents have been observed in the Melanesian basin (Komaki and Kawabe, 2007). In the South Pacific gyre, deeper than 3500 m, O_2 increases to around 190 µmol kg^{-1} due to the intrusion of Lower Circumpolar Deep Water (LCDW) from the southeast (Kawabe and Fujio, 2010). Over the whole transect, O_2 concentrations range from 121 µmol kg^{-1} in the PDW of the Lau basin, to 211 µmol kg^{-1} in the AAIW of the South Pacific gyre (Figure 3A).

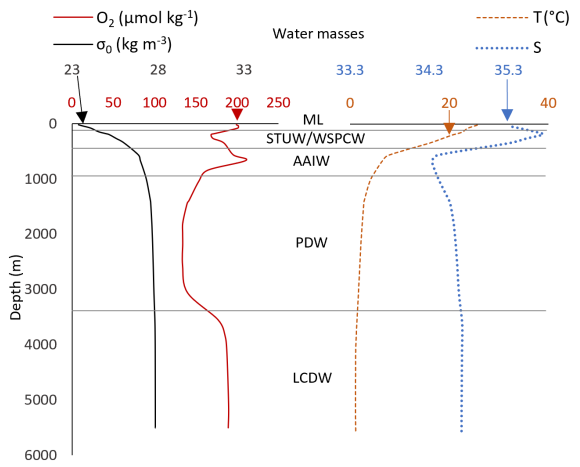

FIGURE 2
Profile of σ_0 (black full line), O_2 (red full line, diamond), T (temperature, orange dash line), and S (salinity, blue dot line) at station 7 with the water mass separations applied in this study, namely the mixed layer (ML), the Subtropical Underwater (STUW), the Western South Pacific Central Water (WSPCW), the Antarctic Intermediate Water (AAIW), the Pacific Deep Water (PDW) and the Lower Circumpolar Deep Water (LCDW). The WSPCW, not present at ST7, is also mentioned to not omit any water mass investigated in this work.

DOC

The distribution and range of DOC concentrations measured in this study are typical to what has been previously reported in the Tropical South Pacific Ocean (e.g., Buck et al., 2018; Fourrier et al., 2022). DOC concentrations ranged from 35 to 80 µM (Figure 3B), with the highest values observed in the mixed layer typical of primary production, ranging from 60 to 80 µM. DOC concentrations decreased with depth due to microbial remineralization to reach typical deep-water values, ranging from 35 to 45 µM in the PDW (and LCDW at stations 7 and 8). Typical deep values are reached within the STUW/WSPCW in line with microbial aerobic respiration at most stations (Figures 2, 3), except at stations 3, 4 and 7, where the concentrations gradient reaches depths of up to 1000 m.

DFe

DFe distribution has been thoroughly described in Tilliette et al. (2022). For the dataset considered in this work, DFe concentrations ranged from 0.13 nM in the mixed layer of the Western Lau basin to 3.13 nM in the mixed layer of the Eastern Lau basin (Figure 4A). Higher DFe concentrations, up to 50 nM, were observed at another location (station 5; Tilliette et al., 2022), however, no data is available for Fe-binding ligand characteristics at this station. The Melanesian basin and the South Pacific gyre show DFe depletion in surface waters attributed to predominant removal processes and limited supply

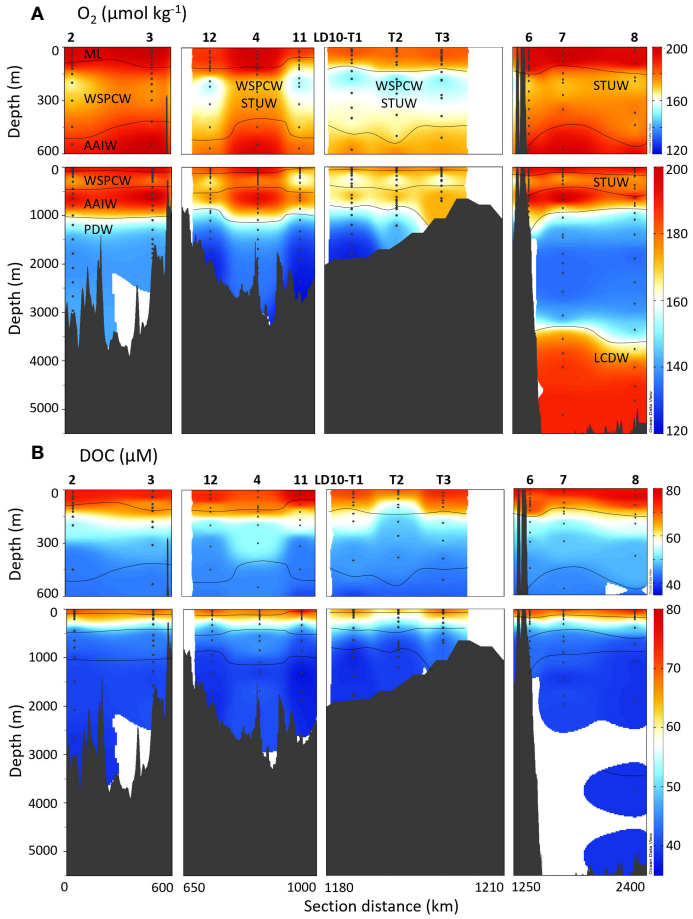

FIGURE 3
Top 600 m and full depth distribution of **(A)** O_2 and **(B)** DOC concentrations for the TONGA cruise (GEOTRACES GPpr14). The approximative water mass boundaries are defined by O_2 (see Figure 2). The section is separated in four segments with, from left to right, the Melanesian basin (stations 2 and 3), the Western Lau basin (stations 12, 4 and 11), the Eastern Lau basin (stations LD10-T1, LD10-T2 and LD10-T3) and the South Pacific gyre (stations 6, 7, and 8). See Figure 1 for more details on the sampling locations.

(Tilliette et al., 2022), and an increase at depth with mineralization in the range of previously reported open-ocean values (e.g., Tagliabue et al., 2012; Resing et al., 2015; Tonnard et al., 2020). The Western Lau basin shows similar DFe depletion in subsurface waters except for an enhancement at station 11 in the WSPCW. Another strong DFe enhancement is observed in the mixed layer of the Eastern Lau basin. The highest values observed in this study are considered to be solely hydrothermal, while deep waters of the Eastern and Western Lau basin show anomalies of DFe enrichment related to either remineralization, island effect, benthic fluxes and/or hydrothermal activity (up to 1.5 nM; Tilliette et al., 2022). Similar concentrations were previously reported for bottom enrichment related to hydrothermal and shelf inputs (e.g. Klunder et al., 2011; Klunder et al., 2012; Resing et al., 2015; Tonnard et al., 2020).

HS-like FDOM

The HS-like FDOM component identified here through EEM/PARAFAC (λ_{Ex1}, $\lambda_{Ex2}/\lambda_{Em}$: 235, 315/436 nm), which are referred to as peaks A + M/C (Coble, 1996; Hudson et al., 2007; Coble et al., 2014) or component 3 (Ishii and Boyer, 2012) in different DOM fluorophore classifications, has been reported in various coastal and marine environments (Ferretto et al., 2017; Tedetti et al., 2020). HS-like FDOM content ranged from 1 QSU in the mixed layer of the Western Lau basin to 4 QSU in the PDW of the Melanesian basin (Figure 4B). HS-like FDOM systematically increased with depth, reflecting its loss by photobleaching or extinction of its fluorescence in the photic layer, and its production in deep waters through the remineralization of organic matter (Nelson et al., 2010; Heller et al., 2013; Yamashita et al., 2017). The depth profiles of HS-like FDOM along the transect (i.e., lower values in surface waters, higher at depth) were thus opposite to those of DOC, a phenomenon already reported for the Atlantic and North Pacific Oceans, as well as at our station 8 in the South Pacific gyre (Omori et al., 2010; Stedmon and Álvarez-Salgado, 2011; Yamashita et al., 2017; Cao et al., 2020; Fourrier et al., 2022). High HS-like FDOM signals were observed in the deep waters at stations 2, 3, 4, LD10-T1, LD10-T2, the highest signal being observed at station 8.

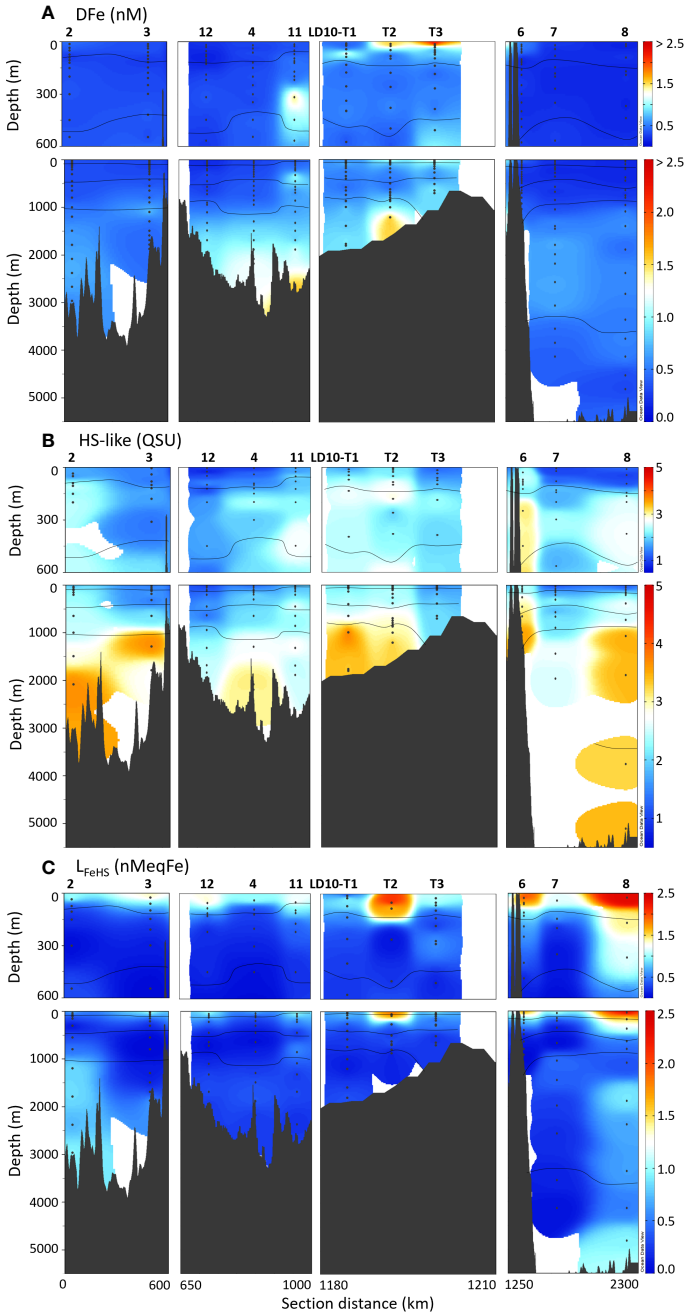

FIGURE 4
Top 600 m and full depth distribution of **(A)** DFe, **(B)** HS-like FDOM and **(C)** L_{FeHS} for the TONGA cruise (GEOTRACES GPpr14). The approximative water mass boundaries are defined by O_2 (see Figures 2, 3A). The section is separated following the description of the studied area (Figure 1).

L_{FeHS}

Details on the distribution and determination of electroactive HS (eHS) in the area during the same cruise are fully described elsewhere (Dulaquais et al., 2023). We show here the eHS determined by complexation with Fe (Dulaquais et al., 2023), referred to as L_{FeHS}, for comparison with HS-like FDOM and Fe-binding ligands (Figure 4C). L_{FeHS} are expressed in nMeqFe following the estimated Fe binding capacity of the fulvic acid standard used (16.4 nmolFe $mgFA^{-1}$; Sukekava et al., 2018). For the dataset considered in this work, L_{FeHS} concentrations ranged from 0.2 to 2.4 nMeqFe with a mean value of 0.6 ± 0.5 nMeqFe (n = 106). The highest values were observed in the mixed layer at all stations and concentrations decreased with depth down to relative minima (between 0.2 and 0.4 nMeqFe) in intermediate waters. Below, in the abyssal waters, concentrations increased again to values higher than 0.6 nMeqFe. Comparatively, high L_{FeHS} concentrations were detected through the entire water column in the oligotrophic waters of the South Pacific gyre collected at station 8 (Fourrier et al., 2022).

Fe-binding ligands

A single class of Fe-binding ligand was detected in all samples, with a mean L_{Fe} of 5.2 ± 1.2 nMeqFe and mean log $K^{cond}_{Fe'L}$ of 11.6 ± 0.4 (n = 103; Figures 5A, C, respectively). Log $K^{cond}_{Fe'L}$ ranged from 10.5 ± 0.2 in the AAIW of the Melanesian basin (station 2) to 12.7 ± 0.3 in the PDW of the Western Lau basin (station 11), encompassing the three ligand classes defined by Gledhill and Buck (2012). As such, 84% of our samples fall in the L_2 class, 13% in the L_1 class, and 4% in the L_3 class. L_{Fe} ranged from 2.8 ± 0.4 nMeqFe in the mixed layer of the Melanesian basin (station 2) to 9.3 ± 1.0 nMeqFe in the PDW of the Melanesian basin (also station 2). The co-occurrence of the maximal and minimal values at the same station illustrates the variability of the processes impacting the DOM in the area, discussed hereafter. High values of L_{Fe} reaching up to 9.0 nMeqFe were observed at two other locations, in the AAIW above the Tonga ridge in the South Pacific gyre (station 6), and in the mixed layer in the Lau basin (station LD 10-T3). At stations 2 and 6, higher L_{Fe} coincided with increased HS-like FDOM (Figure 4B).

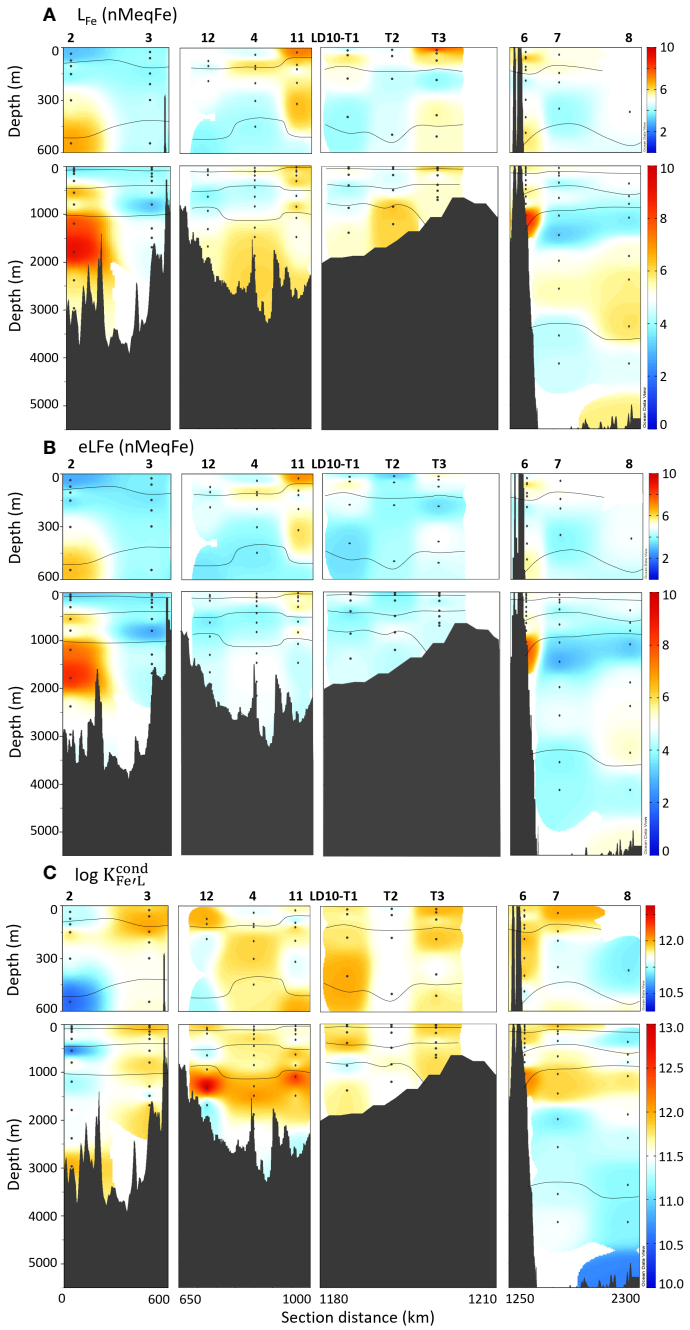

FIGURE 5
Top 600 m and full depth distribution of **(A)** L_{Fe}, **(B)** eL_{Fe} and **(C)** log $K^{cond}_{Fe'L}$ for the TONGA cruise (GEOTRACES GPpr14). The approximative water mass boundaries are defined by O_2 (see Figures 2, 3A). The section is separated following the description of the studied area (Figure 1).

10.3389/fmars.2024.1304118

In all samples, L_{Fe} was present in unusually large excess compared to DFe, with excess ligand (eL_{Fe} = L_{Fe} - DFe) ranging from 2.6 to 8.6 nMeqFe (Figure 5B) and a mean eL_{Fe} of 4.6 ± 1.1 nMeqFe (n = 103).

Fe-binding ligands show relatively constant L_{Fe} and log $K^{cond}_{Fe'L}$ values along water masses and regions over the whole transect (Figure 6), but a few significant differences were observed (Mann-Whitney test, $p< 0.05$; Supplementary Material 2, 3). The significant differences for L_{Fe} were observed between the low values of the mixed layer of the Melanesian basin and the other regions, and between the high values of the PDW and both the mixed layer and the STUW/WSPCW in the Melanesian basin. Log $K^{cond}_{Fe'L}$ was significantly lower in the LCDW in the South Pacific gyre and all other water masses, suggesting specific Fe-binding characteristics of the DOM in this deep water mass.

Discussion

L_{Fe} and log $K^{cond}_{Fe'L}$ distribution in the WTSP

Our eL_{Fe} values (mean = 4.6 ± 1.1 nMeqFe) are c.a. 2.5 times higher than the average reported in the Eastern and Central Tropical South Pacific Oceans (Buck et al., 2018) using exactly the same experimental procedure. The large fraction of eL_{Fe} belonging to the L_2 class throughout the water column suggests a rather homogenous Fe-binding ability of the DOM, while the decreasing DOC concentration along the water column infers a refractory nature of the binding sites and an increase in binding site density with depth. We find that the ligand pool is dominated by L_2 ligands even though we use a high detection window, which can favor detection of the strongest ligands and miss contributions from weaker ligands. In comparison, it was found in the Eastern and Central Tropical South Pacific Oceans that L_1 ligands were generally in excess compared to DFe in the first 1000 m, while excess L_2 and L_3 increased in deeper waters (Buck et al., 2018). The ligand distribution observed in these environments reflects the biological production of strong L_1 in upper waters, and the loss and saturation of these L_1 ligands as DOM is remineralized, resulting in increasing DFe and weaker L_2 and L_3 ligand concentrations in deep waters. In our study, a decrease in log $K^{cond}_{Fe'L}$ with depth was observed in the South Pacific gyre, but without change of ligand class, and no change in log $K^{cond}_{Fe'L}$ in the Melanesian and Lau basins (Figures 5, 6).

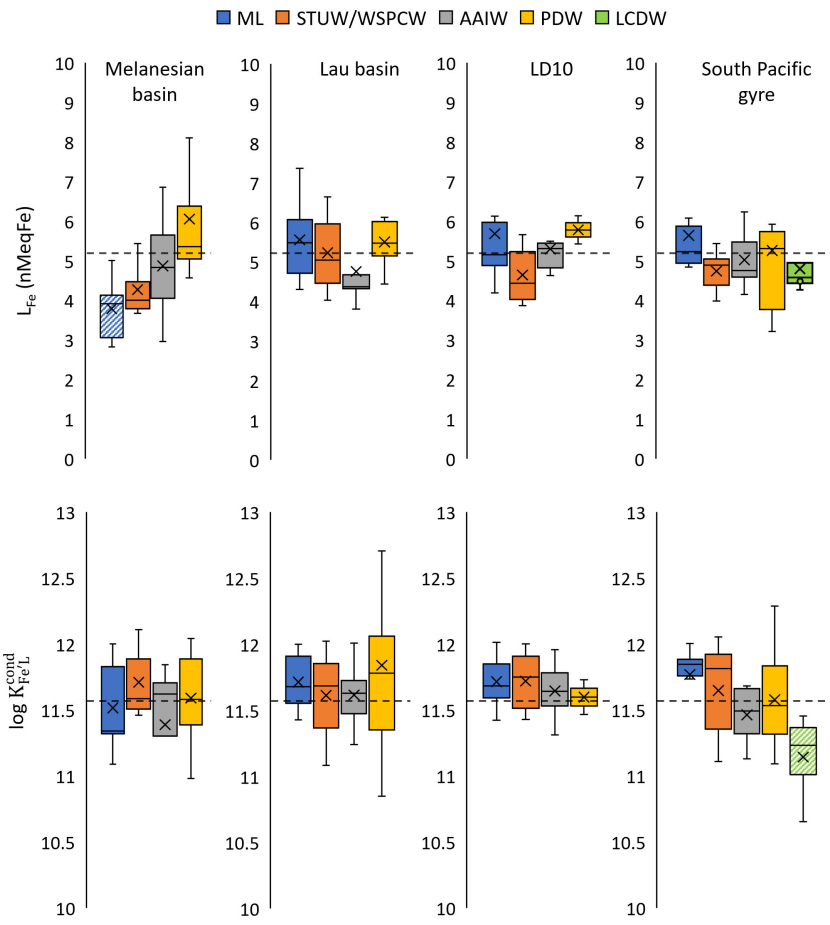

FIGURE 6
Box and Whiskers plots of L_{Fe} and log $K^{cond}_{Fe'L}$ split by the regions and water masses. The mean values of the entire dataset are represented by black dot lines. The hatched boxes correspond to water mass being significantly different compared to the same water mass in other regions (Wilcoxon-Mann-Whitney test, $p < 0.05$). Water mass acronyms can be found in Figures 2, 3A.

The progressive decrease in log $K^{cond}_{Fe'L}$ with increasing depth and increasing distance from the Lau basin gives the impression of a dilution gradient from stronger to weaker ligands into the South Pacific gyre and within the mixed layer of the Melanesian basin (Figures 5, 6, Supplementary Information 3), even though the South Pacific gyre is largely isolated from the Lau basin waters by the Tonga ridge, as seen in DFe and diazotroph abundance (Lory et al., 2022; Tilliette et al., 2022; Figure 4A). Assuming that the DOM produced in the Lau basin has specific Fe-binding ligand properties and it disperses into the Melanesian basin and the South Pacific gyre, it would have to be decoupled from diazotrophic activity and DFe dispersion. This would be in line with previous studies suggesting faster turnover of DFe than Fe-binding ligands, the latter having a much longer residence time (Gerringa et al., 2015; Tagliabue et al., 2023). However, higher resolution is needed to better constrain the spreading of the DOM thought to originate from the recycling of the diazotroph that are thriving in the Lau basin (Bonnet et al., 2023a).

L_{Fe} production for trace metal detoxification

A strong production of L_{Fe} was observed in the surface waters at LD10-T3, related to a hydrothermal input of DFe (Tilliette et al., 2022; Figures 4A, 5B; Table 2). Interestingly, the L_{Fe} enhancement was only detected at the maximum DFe value and did not follow the linear dilution pattern showed by DFe with distance from the hydrothermal vent, suggesting that the amount of hydrothermally-sourced trace metals reached a concentration threshold triggering the production of Fe-binding ligands. The DFe enhancement did not reach toxic levels, therefore, the Fe-binding ligands detected could have been produced by the local plankton communities, including abundant diazotrophs, to neutralize toxic elements and not be Fe-specific/specifically produced to bind Fe. While HS can bind a range of metals, L_{FeHS} and HS-like FDOM did not increase at LD10-T3 (Table 2), and siderophores alone cannot be responsible for the increase in L_{Fe} and DFe since they are usually found at pM concentrations and have higher log $K^{cond}_{Fe'L}$ (Mawji et al., 2008; Bundy et al., 2018; Boiteau et al., 2019). On the other hand, bacterial production of EPS by species collected near hydrothermal vents has been reported as a mechanism for slowing the diffusion of toxic elements into the organism and participating in the scavenging of toxic trace metals (Rougeaux et al., 1996; Nichols et al., 2005; Moppert et al., 2009; Deschatre et al., 2013). Production of EPS showing Fe binding properties was also observed for the nitrogen fixer *Crocosphaera watsonii* collected during the TONGA cruise (C. Lory, unpublished). Our results call for further consideration of the potential implication of EPS for regulating the distribution of the hydrothermally-sourced Fe and other toxic elements in the surface waters of the WTSP Ocean. One must also keep in mind the possible implication of small inorganic forms of Fe to explain the short-distance transport of the DFe enhancement, as highlighted by Dulaquais et al. (2023) and Tagliabue et al. (2023), as well as enhanced scavenging and precipitation in hydrothermally-influenced waters, which may result in ligand unsaturation (Gerringa et al., 2015; Thuroczy et al., 2011).

Both the Melanesian basin and the South Pacific gyre show strong L_{Fe} production in several deep-water samples (Figures 5A, B). On the eastern side of the Tonga ridge, L_{Fe} production coincides with relatively high log $K^{cond}_{Fe'L}$ (Figure 5), high HS-like FDOM (Figure 4) and high tryptophan-like FDOM (Tedetti et al., in prep), while no change in L_{FeHS} nor DFe is apparent (Figure 4). In the Melanesian basin (particularly at station 2), increased L_{Fe} coincides with relatively low log $K^{cond}_{Fe'L}$ (Figure 5), high HS-like FDOM (Figure 4) and high thiol-like compounds (Portlock et al., this issue[2]) and increased L_{FeHS} and DFe (Figure 4). The increased L_{Fe}, thiol-like compounds and tryptophan-like FDOM could be related to the toxicity of hydrothermally sourced metals. Indeed, the production of thiol-like compounds was recently associated with the detoxification of hydrothermal fluid in a ship-board incubation experiment performed with WTSP waters (Tilliette et al., 2023). Regarding the tryptophan-like signal, abiotic processes can lead to the production of tryptophan in hydrothermal systems (Ménez et al., 2018), and benthic interaction could also be involved. More information is required to disentangle the sources of Fe-binding ligands and tryptophan-like FDOM at this location, and efforts should focus on identifying the metals preferentially bound by the DOM associated with hydrothermal activity.

TABLE 2 Values in surface samples (depth < 20 m) with distance from the hydrothermal site.

	LD10-T1 – 15 km	LD10-T2 – 8 km	LD10-T3 – 2 km
DFe (nM)	0.38	1.52	3.20
L_{Fe} (nMeqFe)	4.2 ± 0.6	4.7 ± 0.9	8.8 ± 0.7
log K^{cond}_{FeL}	11.8 ± 0.2	11.4 ± 0.3	11.9 ± 0.2
L_{FeHS} (nMeqFe)	1.2	2.2	1.1
HS-like FDOM (QSU)	1.8	2.1	1.3

Humic contribution to DFe stabilization and to the Fe-binding ligand pool

Previous studies have also found L_2 ligands to dominate the water column in the South Tropical Pacific (e.g., Buck et al., 2018; Cabanes et al., 2020). The L_2 ligand class is often considered to be humic-like (Gledhill and Buck, 2012; Hassler et al., 2017), and our averaged log $K^{cond}_{Fe'L}$ of 11.6 ± 0.4 corresponds to log $K^{cond}_{Fe'L}$ values reported for Suwannee River humic-acid standards (SRHA; 11.1-11.6; Laglera and van den Berg, 2009; Abualhaija and van den Berg, 2014; Abualhaija et al., 2015). While there was no correlation of Fe-

2 Portlock, G., Tilliette, C., Bonnet, S., Guieu, C., Whitby, H., and Salaun, P. Distribution and behaviour of reduced sulphur substances in the oligotrophic and hydrothermal waters of the Western South Tropical Pacific.

binding ligands with any parameters considered in this study, DFe showed the strongest correlation with HS-like FDOM (Table 3). Both DFe and HS-like FDOM increased in deep waters, with DFe being possibly complexed by HS-like FDOM as Fe(II) and/or Fe (III). Indeed, HS-like FDOM have been reported in hydrothermal fluids and are potentially capable of stabilizing Fe(II) (Yang et al., 2012; Sarma et al., 2018). However, it is not possible to estimate the proportion of L_{Fe} represented by the HS-like FDOM; for this, fluorescence quenching experiments, consisting of titrating the fluorophore with DFe, could be considered in future studies (Chen et al., 1994; Ohno et al., 2008).

The fluorescent and electroactive components of HS are thought to overlap, but the electroactive fraction of humic material, L_{FeHS} which comprises around 5% of the DOC in deep waters (Laglera and van den Berg, 2009; Dulaquais et al., 2018; Fourrier et al., 2022; Dulaquais et al., 2023), is thought to represent the metal-binding fraction specifically and can be compared to ligand concentrations directly. LFeHS have been shown to compose a large fraction of the Fe-binding ligands supplied during remineralisation (Whitby et al. 2020a). DFe has been shown to correlate with L_{FeHS} in some oceanic regions (Dulaquais et al., 2018; Laglera et al., 2019; Whitby et al., 2020b), and with AOU and HS-like FDOM in the Arctic and North Pacific Oceans (Tani et al., 2003; Hioki et al., 2014; Yamashita et al., 2017; Cao et al., 2020). On the other hand, DFe, L_{Fe}, L_{FeHS} and HS-like FDOM tend not to correlate in the Atlantic Ocean (Heller et al., 2013; Whitby et al., 2020b). The electroactive and fluorescent properties of HS have been thoroughly investigated at station 8 of the TONGA cruise (Fourrier et al., 2022), but in hydrothermal systems, the contribution of L_{FeHS} and HS-like FDOM to the Fe-binding ligand pool and DFe transport is currently unknown.

Here, L_{FeHS} represented 20 ± 13% of L_{Fe} in the mixed layer, and 8 ± 6% in deep waters (Table 1; error calculated with L_{FeHS} standard deviation); therefore, while the average log $K^{cond}_{Fe'L}$ across the samples is consistent with humic complexation, and DFe correlates well with humic-like FDOM, electroactive L_{FeHS} specifically do not dominate the Fe-binding ligand pool. While this may seem unexpected, this % contribution to L_{Fe} is similar to previous studies in the Pacific (2-51%; Cabanes et al., 2020; Whitby et al., 2020b), which tends to have a lower contribution of L_{FeHS} to the total ligand pool than in other ocean basins [e.g. L_{FeHS} comprise ~20-60% of the ligand pool in the Atlantic and Mediterranean (Dulaquais et al., 2018; Whitby et al., 2020b) and almost all of the ligand pool in parts of the Arctic Ocean (Slagter et al., 2017)]. While a large fraction of the ligand pool is not associated with electroactive HS, the L_{FeHS} that are present play an important role in Fe complexation, actively complexing around 30% of the DFe in these samples (Dulaquais et al., 2023).

Comparing the carbon content of the FA standard to DOC concentrations, L_{FeHS} represented 4.6 ± 2.6% of the DOC in the mixed layer (n = 17), and 2.2 ± 1.7% in deep waters (n = 60), similar to previously reported ranges (2 to 5%; Laglera and van den Berg, 2009; Dulaquais et al., 2018). While other, non-humic ligand groups may be contributing to the high L_{Fe}, the low correlation of L_{FeHS} with DFe, DOC, and AOU could be an indication of intense *in-situ* production of non-electroactive HS, corroborated by the low negative correlation between L_{FeHS} and HS-like FDOM (Table 3), characteristic of microbial respiration (Fourrier et al., 2022). Other metals can compete with Fe for L_{FeHS} complexation (e.g., Yang and van den Berg, 2009; Abualhaija and van den Berg, 2014; Whitby and van den Berg, 2015) and can also impact the HS-like FDOM (Zhao and Nelson, 2005). Non-specific ligands which contribute to L_{Fe} but can complex other metals could explain the unsaturation of the Fe-binding ligands produced in the Lau basin. The effect of competitive metals on Fe-binding ability of ligands, L_{FeHS} and HS-like FDOM would need to be investigated to better understand their potential impact on Fe speciation and cycling in hydrothermal environments.

Suggestions for future CLE-AdCSV studies

Toward tracing DOM characteristics with the reduction potential of the $FeSA_2$ complex

During AdCSV analyses, a variation in the peak potential of the reduction of the Fe-added ligand complex ($FeSA_2$) was

TABLE 3 Table of the Spearman rank correlation (ρ) of investigated parameters in this study.

	AOU (µM)	DOC (µM)	DFe (µM)	eL_{Fe} (nMeqFe)	log $K^{cond}_{Fe''L}$	L_{FeHS} (nMeqFe)
DOC (µM)	**-0.93 n = 161**					
DFe (µM)	**0.52 n = 238**	**-0.50 n = 151**				
eL_{Fe} (nMeqFe)	0.07 n = 103	0.00 n = 66	0.09 n = 103			
log K^{cond}_{FeL}	-0.18 n = 103	0.12 n = 66	-0.08 n = 103	-0.18 n = 103		
L_{FeHS} (nMeqFe)	-0.47 n = 120	0.46 n = 79	-0.23 n = 119	-0.05 n = 94	0.11 n = 94	
HS-like FDOM (QSU)	**0.71 n = 130**	**-0.73 n = 124**	**0.45 n = 116**	-0.03 n = 50	-0.17 n = 50	-0.26 n = 61

Blue corresponds to negative correlation, red to positive correlation, and white to absence of correlation. The intensity of the color is proportional to the strength of the correlation. Bold values correspond to p< 0.0001.

observed along the water column. The $FeSA_2$ peak potential ranged from -413 mV to -445 mV within the first 200 m (well-oxygenated mixed layer and most of the STUW/WSPCW), then decreased with depth to 1200 m where it reached a stable mean value of -473 mV down to the most abyssal waters (Figure 7). Also, in the mixed layer, the peak potential was significantly different between the Melanesian basin, the Lau basin, and the South Pacific gyre (Mann-Whitney test, $p< 0.05$; Supplementary Information 3). We hypothesize that the shift in reduction potential was due to an electroactive fraction of the DOM produced in the surface waters in the area. Indeed, the reduction of the metal complexed by the added ligand during AdCSV analysis happens at a specific potential following the Nernst equation (Nernst, 1889). The value of this potential is driven by i) the conditions of temperature, pH, and salinity, ii) the activity of the redox species, iii) the experimental conditions such as stripping scan rate, pulse time and pulse amplitude and iv) the adsorbed layer of organics accumulated on the electrode surface during the deposition step. Here, the temperature in the laboratory was controlled, the pH fixed by the addition of a buffer, and no correlation was found between the reduction potential and the salinity. The experimental measuring conditions were kept the same. The CLE-AdCSV method using SA takes advantage of a catalytic loop involving the reduction of the dissolved O_2 to hydrogen peroxide which immediately re-oxidize Fe(II) back into Fe(III), allowing for multiple reductions of the same ion and enhancing the signal (Laglera et al., 2016; Mahieu, 2023). The samples were equilibrated with air in the voltametric cell, ensuring a constant oxygen concentration (Mahieu, 2023) and a similar catalytic effect, regardless of the sample being analyzed. AdCSV analysis includes an accumulation step at a positive potential where the electroactive complex $FeSA_2$ adsorbs at the electrode surface prior to its stripping. During this stripping, other compounds, organic and inorganic, may adsorb at the electrode surface and may impact the stripping peak potential. The influence of the DOM composition on the peak potential of $FeSA_2$ is yet to be addressed, but the ubiquity of the peak shift suggests similar electroactive DOM in the surface waters of all basins of the WTSP. It will be interesting to assess whether it is possible to identify specific components of DOM by the shift in the peak potential. Overall, this observation could highlight a novel way to identify changes in DOM composition, but it requires further investigation.

Analytical constraints for Fe-binding ligand detection by CLE-AdCSV

There are different CLE-AdCSV methodologies currently in use to evaluate the role of DOM complexation in DFe stabilization and transport. Although all are valuable, they are difficult to compare because of the specificities (e.g. detection window) of each method. Several basin scale investigations have presented Fe organic speciation in the WTSP, but they were obtained using different experimental procedure which might explain some of the observed differences. Using TAC as added ligand, Kondo et al. (2012) reported in most samples a low eL_{Fe} (< 1 nMeqFe) in the L_1 ligand class. In contrast, other studies in the Pacific Ocean using the added ligand SA showed ubiquitous, large eL_{Fe} (> 1 nMeqFe) falling in the L_2 class (Buck et al., 2018; Cabanes et al., 2020; this study). The difference can be explained by the analytical conditions with a higher detection window ($\alpha_{Fe'AL}$) for TAC than for SA, meaning that titrations with TAC focus on fewer Fe-binding ligands of

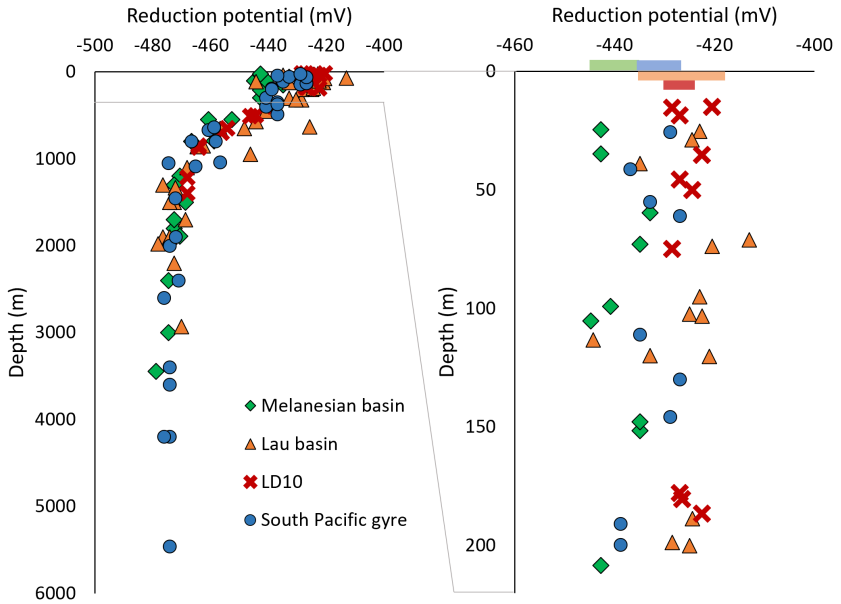

FIGURE 7
Reduction potential of the FeSA peak with depth for the entire water column (left) and the top 200 m (right), with the standard deviation centered on the averaged value for the first 200 m represented by colored bar.

higher log $K^{cond}_{Fe'L}$ than the titrations with SA. The difference in detection window could lead to the underestimation of the HS-like contribution to the ligand pool because of the absence of competition with TAC (Laglera et al., 2011).

The analyses presented in this study were all performed in the dissolved fraction, without discrimination of the soluble and colloidal size fraction. Metal-binding compounds in the soluble Fe fraction (< 0.02 µm) are assumed to be mostly organic, while the colloidal fraction (0.02 to 0.2 µm, or 0.45 µm here) may be composed of a wider mix of organic and inorganic compounds. It was suggested that this colloidal fraction of Fe was essential for DFe transport in the Subarctic Pacific (Kondo et al., 2021). Similarly, knowledge of the size fractionation of DFe, Fe-binding ligands, and HS partitioning in the Lau basin would greatly help better understand DFe speciation in this very dynamic region.

Accurate DFe concentrations are required in the calculation of L_{Fe} and log $K^{cond}_{Fe'L}$. Compared to mid-ocean ridges, volcanic arcs are characterized by higher carbon dioxide (CO_2), sulfur dioxide (SO_2) and hydrogen sulfide (H_2S) enrichments, responsible for increased DFe removal by the formation of Fe-sulfide and Fe-oxyhydroxides along the dilution of hydrothermal plumes (e.g., Field and Sherrell, 2000). Such gas enrichment and DFe removal have been observed at several locations along the Tonga-Kermadec volcanic arc (Massoth et al., 2003; de Ronde et al., 2007; Resing et al., 2011; Neuholz et al., 2020; Kleint et al., 2022). The presence of such inorganic colloidal material can be problematic because DFe may be released under the acidic conditions used for DFe determination while being possibly inert species for CLE-AdCSV, which is performed at natural pH. The net effect is therefore an overestimation of the effective DFe concentration, leading to biased L_{Fe} and log $K^{cond}_{Fe'L}$. It is known for instance that the crystalline structure of some Fe-oxyhydroxides can sterically isolate Fe from metal-binding ligands (Kraemer et al., 2005; Dulaquais et al., 2023) while dissolving in acidic conditions (Liu and Millero, 2002). This effect has been observed in hydrothermal plumes by Kleint et al. (2016). They showed that up to 90% of DFe determined in acidified samples was non-labile to their added ligand in the buoyant plume, but this value was down to 15% in the non-buoyant plume. It is worth noting that the hydrothermal fluids investigated by Kleint et al. (2016) had DFe concentrations in the µM range, so the overestimation of DFe had a considerable impact on L_{Fe} and log $K^{cond}_{Fe'L}$ calculations. In the transect presented here, the most hydrothermally-influenced station was still 2km away from the vent and 90% of DFe concentrations were< 1 nM, which represents no more than 20% of the average L_{Fe} measured for our dataset. Thus, the error related to the potential overestimation of DFe is negligible for most of our samples. Nevertheless, the impact on CLE-AdCSV titrations of sulfides, oxyhydroxides and other aggregate materials filtered and classified as dissolved by the traditional operational definition is not known, and the competition between binding with the added ligand and adsorption/binding with inorganic and colloidal material is unknown.

The increasing number of Fe-binding ligand investigations in hydrothermal systems have encompassed a variety of techniques, each with advantages and disadvantages. Kleint et al. (2016) highlighted the issue related to the accurate definition of DFe concentration with SA within the hydrothermal plume in the Lau basin, and Wang et al. (2022) presented the correlation of the Fe isotopic ratios with the log $K^{cond}_{Fe'L}$ defined by reversed CLE-AdCSV using 1-nitroso-2-napthol (NN). Here, we present the distribution of the Fe-binding ligands in the Lau Basin and adjacent waters using SA. The next step forward in the characterization of hydrothermally derived Fe-binding ligands could be to directly compare the different available electroanalytical methods on the same water samples.

Conclusion

The TONGA transect (GPpr14) revealed intense production and accumulation of Fe-binding ligands predominantly of intermediate log $K^{cond}_{Fe'L}$ at all stations. The high L_{Fe} and eL_{Fe} observed in the area contrast with similar regions and may originate from the unusually high diazotroph activity known to occur in the Lau basin. Limited stabilization of the hydrothermally-sourced DFe is most likely explained by competition from other metals and non-specificity of the ligands being produced, further supported by companion studies that report high levels of reduced sulfur substances and humic-like FDOM that coincide with our high L_{Fe} (in prep.). These non-specific ligands could be a detoxification response to hydrothermal waters, a hypothesis supported by ship-board incubation experiments (Tilliette et al., 2023).

Around 30% of DFe in these samples is within humic complexes (Dulaquais et al., 2023) and good agreement between FDOM and DFe suggest possible stabilization of a fraction of DFe as Fe(II) by HS-like FDOM. However, while the average log $K^{cond}_{Fe'L}$ was consistent with humic complexation across the ligand pool, ligands were in great excess of DFe and electroactive L_{FeHS} accounted for only 20 ± 13% of L_{Fe} in the mixed layer and 8 ± 6% in deep waters. Different trends in L_{FeHS} and HS-like FDOM distributions confirm that HS-like FDOM and L_{FeHS} account for overlapping yet distinct fractions of the humic pool, and that the electroactive fraction of humics may underestimate the role of humic material in metal complexation. We recommend the use of quenching experiments in samples collected in the WTSP to evaluate the role of the HS-like FDOM in DFe transport and in Fe-binding ligand composition in future studies. Other ligands such as EPS and siderophores likely also contributed to Fe complexation, although the average log $K^{cond}_{Fe'L}$ values suggest strong ligands such as siderophores were also not a dominant component of the ligand pool. Our results may also be explained by competition between metals for non-specific ligands, and a multi-metal approach to examine the affinity of the binding sites of humic nature toward hydrothermally sourced trace metals would provide further insight. Ultimately, the partitioning of DFe, Fe-binding ligands, L_{FeHS} and HS-like FDOM should be investigated in both the soluble and colloidal fractions, and include the characterization of EPS, siderophores and other potential ligands.

The Tonga ridge effectively isolates the South Pacific gyre from the Lau basin, and yet there was an apparent dilution gradient from stronger to weaker ligands from the Lau basin into the South Pacific

gyre and within the mixed layer of the Melanesian basin. This gradient was also seen in the electrochemical potential of the $FeSA_2$ peak in the mixed layer, which was highest in the Lau basin and decreased in adjacent surface waters of the Melanesian basin and South Pacific gyre. To our knowledge, this is the first time that a change in peak potential associated with changes in sample composition has been reported. We hypothesize that the peak shift could present a novel way to identify specific components of DOM, but this requires further investigation. In view of the existing studies harnessing a combination of forward and reverse titrations and different added ligands to determine Fe speciation in the WTSP, this region could present an ideal location for further intercomparison efforts to evaluate the ability of CLE-AdCSV in characterizing Fe-binding ligands of hydrothermal origin.

Data availability statement

The original contributions presented in the study are included in the article/Supplementary Material. Further inquiries can be directed to the corresponding author.

Author contributions

LM: Formal Analysis, Investigation, Writing – original draft. HW: Supervision, Writing – review & editing. GD: Formal Analysis, Writing – review & editing. CT: Formal Analysis, Writing – review & editing. CaG: Formal Analysis, Writing – review & editing. MT: Formal Analysis, Writing – review & editing. DL: Formal Analysis, Writing – review & editing. PF: Formal Analysis, Writing – review & editing. MB: Writing – review & editing. GS: Writing – review & editing. SB: Writing – review & editing. CéG: Writing – review & editing. PS: Supervision, Writing – review & editing.

Funding

The author(s) declare financial support was received for the research, authorship, and/or publication of this article. The work contained in this paper was conducted during a PhD study supported by the Natural Environment Research Council (NERC) EAO Doctoral Training Partnership and is fully-funded by NERC whose support is gratefully acknowledged (grant NE/L002469/1). This work is a contribution to the TONGA project (Shallow hydroThermal sOurces of trace elemeNts: potential impacts on biological productivity and the bioloGicAl carbon pump). The TONGA cruise (GEOTRACES GPpr14, November 2019, https://doi.org/10.17600/18000884) was funded by the TGIR Flotte Océanographique Française, the A-MIDeX foundation of the Aix-Marseille University, the LEFE-CYBER and GMMC programs and the ANR (grant TONGA ANR-18- CE01-0016). This work was partially supported by the "PHC Alliance" programme, funded by the UK Department for Business, Energy & Industrial Strategy (now DSIT), the French Ministry for Europe and Foreign Affairs, and the French Ministry of Higher Education, Research and Innovation.

Acknowledgments

We warmly thank all the scientists, the captain, and the crew of the R/V L'Atalante for their cooperative work at sea during the TONGA cruise. We also thank V. Taillander for the CTD acquisition and data treatment, and D. Gonzales-Santana, M-E Vorrath, members of the trace metal sampling team. We also thank K. Buck for the valuable comments and discussion during the preparation of the manuscript.

Conflict of interest

The authors declare that the research was conducted in the absence of any commercial or financial relationships that could be construed as a potential conflict of interest.

Publisher's note

Supplementary material

The Supplementary Material for this article can be found online at: https://www.frontiersin.org/articles/10.3389/fmars.2024.1304118/full#supplementary-material

References

Abualhaija, M. M., and van den Berg, C. M. G. (2014). Chemical speciation of iron in seawater using catalytic cathodic stripping voltammetry with ligand competition against salicylaldoxime. *Mar. Chem.* 164, 60–74. doi: 10.1016/j.marchem.2014.06.005

Abualhaija, M. M., Whitby, H., and van den Berg, C. M. G. (2015). Competition between copper and iron for humic ligands in estuarine waters. *Mar. Chem.* 172, 46–56. doi: 10.1016/j.marchem.2014.06.00510.1016/j.marchem.2015.03.010

Barbeau, K., Rue, E. L., Bruland, K. W., and Butler, A. (2001). Photochemical cycling of iron in the surface ocean mediated by microbial iron(iii)-binding ligands. *Nature* 413, 409–413. doi: 10.1038/35096545

Bennett, S. A., Achterberg, E. P., Connelly, D. P., Statham, P. J., Fones, G. R., and German, C. R. (2008). The distribution and stabilisation of dissolved Fe in deep-sea hydrothermal plumes. *Earth Planetary Sci. Lett.* 270 (3-4,), 157–167. doi: 10.1016/j.epsl.2008.01.048

Boiteau, R. M., and Repeta, D. J. (2022). Slow kinetics of iron binding to marine ligands in seawater measured by isotope exchange liquid chromatography-inductively coupled plasma mass spectrometry. *Environ. Sci. Technol.* 56, 3770–3779. doi: 10.1021/acs.est.1c06922

Boiteau, R. M., Till, C. P., Coale, T. H., Fitzsimmons, J. N., Bruland, K. W., and Repeta, D. J. (2019). Patterns of iron and siderophore distributions across the California Current System. *Limnology Oceanography* 64, 376–389. doi: 10.1002/lno.11046

Bonnet, S., Benavides, M., Le Moigne, F. A. C., Camps, M., Torremocha, A., Grosso, O., et al. (2023a). Diazotrophs are overlooked contributors to carbon and nitrogen export to the deep ocean. *ISME J.* 17, 47–58. doi: 10.1038/s41396-022-01319-3

Bonnet, S., Caffin, M., Berthelot, H., Grosso, O., Benavides, M., Helias-Nunige, S., et al. (2018). In-depth characterization of diazotroph activity across the western tropical South Pacific hotspot of N2 fixation (OUTPACE cruise). *Biogeosciences* 15, 4215–4232. doi: 10.5194/bg-15-4215-2018

Bonnet, S., Caffin, M., Berthelot, H., and Moutin, T. (2017). Hot spot of N2 fixation in the western tropical South Pacific pleads for a spatial decoupling between N2 fixation and denitrification. *Proc. Natl. Acad. Sci.* 114, E2800–E2801. doi: 10.1073/pnas.1619514114

Bonnet, S., Guieu, C., Taillandier, V., Boulart, C., Bouruet-Aubertot, P., Gazeau, F., et al. (2023b). Natural iron fertilization by shallow hydrothermal sources fuels diazotroph blooms in the ocean. *Science* 380, 812–817. doi: 10.1126/science.abq4654

Boyd, P. W., Ibisanmi, E., Sander, S. G., Hunter, K. A., and Jackson, G. A. (2010). Remineralization of upper ocean particles: Implications for iron biogeochemistry. *Limnology Oceanography* 55, 1271–1288. doi: 10.4319/lo.2010.55.3.1271

Boyd, P. W., and Tagliabue, A. (2015). Using the L* concept to explore controls on the relationship between paired ligand and dissolved iron concentrations in the ocean. *Mar. Chem. SCOR WG 139: Organic Ligands A Key Control Trace Metal Biogeochem. Ocean* 173, 52–66. doi: 10.1016/j.marchem.2014.12.003

Browning, T. J., and Moore, C. M. (2023). Global analysis of ocean phytoplankton nutrient limitation reveals high prevalence of co-limitation. *Nat. Commun.* 14, 5014. doi: 10.1038/s41467-023-40774-0

Buck, K. N., Lohan, M. C., Berger, C. J. M., and Bruland, K. W. (2007). Dissolved iron speciation in two distinct river plumes and an estuary: Implications for riverine iron supply. *Limnol. Oceanogr.* 52, 843–855. doi: 10.4319/lo.2007.52.2.0843

Buck, K. N., Sedwick, P. N., Sohst, B., and Carlson, C. A. (2018). Organic complexation of iron in the eastern tropical South Pacific: Results from US GEOTRACES Eastern Pacific Zonal Transect (GEOTRACES cruise GP16). *Mar. Chem. U.S. GEOTRACES Eastern Trop. Pacific Transect (GP16)* 201, 229–241. doi: 10.1016/j.marchem.2017.11.007

Buck, K. N., Sohst, B., and Sedwick, P. N. (2015). The organic complexation of dissolved iron along the U.S. GEOTRACES (GA03) North Atlantic Section. *Deep Sea Res. Part II Top. Stud. Oceanogr.* 116, 152–165. doi: 10.1016/j.dsr2.2014.11.016

Bundy, R. M., Boiteau, R. M., McLean, C., Turk-Kubo, K. A., McIlvin, M. R., Saito, M. A., et al. (2018). Distinct siderophores contribute to iron cycling in the mesopelagic at station ALOHA. *Front. Mar. Sci.* 5. doi: 10.3389/fmars.2018.00061

Bundy, R. M., Jiang, M., Carter, M., and Barbeau, K. A. (2016). Iron-binding ligands in the southern california current system: mechanistic studies. *Front. Mar. Sci.* 3. doi: 10.3389/fmars.2016.00027

Cabanes, D. J. E., Norman, L., Bowie, A. R., Strmečki, S., and Hassler, C. S. (2020). Electrochemical evaluation of iron-binding ligands along the Australian GEOTRACES southwestern Pacific section (GP13). *Mar. Chem.* 219, 103736. doi: 10.1016/j.marchem.2019.103736

Cao, F., Zhu, Y., Kieber, D. J., and Miller, W. L. (2020). Distribution and photoreactivity of chromophoric and fluorescent dissolved organic matter in the Northeastern North Pacific Ocean. *Deep Sea Res. Part Oceanogr. Res. Pap.* 155, 103168. doi: 10.1016/j.dsr.2019.103168

Carpenter, J. H. (1965). The accuracy of the winkler method for dissolved oxygen analysis1. *Limnol. Oceanogr.* 10, 135–140. doi: 10.4319/lo.1965.10.1.0135

Carritt, D. E., and Carpenter, J. H. (1966). Comparison and evaluation of currently employed modifications of the Winkler method for determining dissolved oxygen in sea-water; a NASCO report. *J. Mar. Res.* 24, 286–318.

Cheize, M., Sarthou, G., Croot, P. L., Bucciarelli, E., Baudoux, A.-C., and Baker, A. R. (2012). Iron organic speciation determination in rainwater using cathodic stripping voltammetry. *Analytica Chim. Acta* 736, 45–54. doi: 10.1016/j.aca.2012.05.011

Chen, Y., Jurkevitch, E., Bar-Ness, E., and Hadar, Y. (1994). Stability constants of pseudobactin complexes with transition metals. *Soil Sci. Soc. America J.* 58, 390–396. doi: 10.2136/sssaj1994.03615995005800020021x

Coble, P. G. (1996). Characterization of marine and terrestrial DOM in seawater using excitation-emission matrix spectroscopy. *Mar. Chem.* 51, 325–346. doi: 10.1016/0304-4203(95)00062-3

Coble, P. G., Lead, J., Baker, A., Reynolds, D. M., and Spencer, R. G. M. (2014). *Aquatic Organic Matter Fluorescence* (New York, USA: Cambridge University Press).

Cordero, O. X., Ventouras, L.-A., DeLong, E. F., and Polz, M. F. (2012). Public good dynamics drive evolution of iron acquisition strategies in natural bacterioplankton populations. *Proc. Natl. Acad. Sci.* 109, 20059–20064. doi: 10.1073/pnas.1213344109

Croot, P. L., Andersson, K., Öztürk, M., and Turner, D. R. (2004). The distribution and speciation of iron along 6°E in the Southern Ocean. *Deep Sea Res. Part II: Topical Stud. Oceanography SWEDARP 1997/98 Expedition* 51, 2857–2879. doi: 10.1016/j.dsr2.2003.10.012

Cutter, G. A., Casciotti, K., Croot., P. L., Heimburger, L.-E., Lohan, M., Planquette, H., et al. (2017). *Sampling and sample-handling protocols for GEOTRACES cruises, Version 3*. Available at: https://epic.awi.de/id/eprint/51363/1/Cookbook.pdf.

de Ronde, C. E. J., Baker, E. T., Massoth, G. J., Lupton, J. E., Wright, I. C., Sparks, R. J., et al. (2007). Submarine hydrothermal activity along the mid-Kermadec Arc, New Zealand: Large-scale effects on venting. *Geochem. Geophys. Geosyst.* 8, Q07007. doi: 10.1029/2006GC001495

Deschatre, M., Ghillebaert, F., Guezennec, J., and Colin, C. S. (2013). Sorption of copper(II) and silver(I) by four bacterial exopolysaccharides. *Appl. Biochem. Biotechnol.* 171, 1313–1327. doi: 10.1007/s12010-013-0343-7

Dittmar, T., Lennartz, S. T., Buck-Wiese, H., Hansell, D. A., Santinelli, C., Vanni, C., et al. (2021). Enigmatic persistence of dissolved organic matter in the ocean. *Nat. Rev. Earth Environ.* 2, 570–583. doi: 10.1038/s43017-021-00183-7

Dulaquais, G., Fourrier, P., Guieu, C., Mahieu, L., Riso, R., Salaun, P., et al. (2023). The role of humic type ligands in the bioavailability and stabilization of dissolved iron in the Western Tropical South Pacific Ocean. *Front. Mar. Sci.* 10, 19. doi: 10.3389/fmars.2023.1219594

Dulaquais, G., Waeles, M., Gerringa, L. J. A., Middag, R., Rijkenberg, M. J. A., and Riso, R. (2018). The biogeochemistry of electroactive humic substances and its connection to iron chemistry in the north east atlantic and the western mediterranean sea. *J. Geophys. Res. Oceans* 123, 5481–5499. doi: 10.1029/2018JC014211

Ferretto, N., Tedetti, M., Guigue, C., Mounier, S., Raimbault, P., and Goutx, M. (2017). Spatio-temporal variability of fluorescent dissolved organic matter in the Rhône River delta and the Fos-Marseille marine area (NW Mediterranean Sea, France). *Environ. Sci. Pollut. Res.* 24, 4973–4989. doi: 10.1007/s11356-016-8255-z

Field, M. P., and Sherrell, R. M. (2000). Dissolved and particulate Fe in a hydrothermal plume at 9°45′N, East Pacific Rise:: Slow Fe (II) oxidation kinetics in Pacific plumes. *Geochim. Cosmochim. Acta* 64, 619–628. doi: 10.1016/S0016-7037(99)00333-6

Fourrier, P., Dulaquais, G., Guigue, C., Giamarchi, P., Sarthou, G., Whitby, H., et al. (2022). Characterization of the vertical size distribution, composition and chemical properties of dissolved organic matter in the (ultra)oligotrophic Pacific Ocean through a multi-detection approach. *Mar. Chem.* 240, 104068. doi: 10.1016/j.marchem.2021.104068

Garcia, H. E., and Gordon, L. I. (1992). Oxygen solubility in seawater: Better fitting equations. *Limnol. Oceanogr.* 37, 1307–1312. doi: 10.4319/lo.1992.37.6.1307

Genovese, C., Grotti, M., Pittaluga, J., Ardini, F., Janssens, J., Wuttig, K., et al. (2018). Influence of organic complexation on dissolved iron distribution in East Antarctic pack ice. *Mar. Chem.* 203, 28–37. doi: 10.1016/j.marchem.2018.04.005

German, C. R., Baker, E. T., Connelly, D. P., Lupton, J. E., Resing, J., Prien, R. D., et al. (2006). Hydrothermal exploration of the fonualei rift and spreading center and the northeast lau spreading center. *Geochem. Geophys. Geosyst.* 7 (11). doi: 10.1029/2006GC001324

Gerringa, L. J. A., Rijkenberg, M. J. A., Schoemann, V., Laan, P., and de Baar, H. J. W. (2015). Organic complexation of iron in the West Atlantic Ocean. *Mar. Chem. Cycles Metals Carbon Oceans A Tribute Work Stimulated Hein Baar* 177, 434–446. doi: 10.1016/j.marchem.2015.04.007

Gerringa, L. J. A., Rijkenberg, M. J. A., Thuróczy, C.-E., and Maas, L. R. M. (2014). A critical look at the calculation of the binding characteristics and concentration of iron complexing ligands in seawater with suggested improvements. *Environ. Chem.* 11, 114–136. doi: 10.1071/EN13072

Gerringa, L. J. A., Veldhuis, M. J. W., Timmermans, K. R., Sarthou, G., and de Baar, H. J. W. (2006). Co-variance of dissolved Fe-binding ligands with phytoplankton characteristics in the Canary Basin. *Mar. Chem.* 102, 276–290. doi: 10.1016/j.marchem.2006.05.004

Gledhill, M., and Buck, K. N. (2012). The organic complexation of iron in the marine environment: A review. *Front. Microbiol.* 3. doi: 10.3389/fmicb.2012.00069

Gledhill, M., and van den Berg, C. M. G. (1994). Determination of complexation of iron(III) with natural organic complexing ligands in seawater using cathodic stripping voltammetry. *Mar. Chem.* 47, 41–54. doi: 10.1016/0304-4203(94)90012-4

Gledhill, M., Zhu, K., Rusiecka, D., and Achterberg, E. P. (2022). Competitive interactions between microbial siderophores and humic-like binding sites in european shelf sea waters. *Front. Mar. Sci.* 9. doi: 10.3389/fmars.2022.855009

González, A. G., Bianco, A., Boutorh, J., Cheize, M., Mailhot, G., Delort, A.-M., et al. (2022). Influence of strong iron-binding ligands on cloud water oxidant capacity. *Sci. Total Environ.* 829, 154642. doi: 10.1016/j.scitotenv.2022.154642

González, A. G., Cadena-Aizaga, M. I., Sarthou, G., González-Dávila, M., and Santana-Casiano, J. M. (2019). Iron complexation by phenolic ligands in seawater. *Chem. Geol.* 511, 380–388. doi: 10.1016/j.chemgeo.2018.10.017

Guieu, C., and Bonnet, S. (2019). *TONGA 2019 cruise, L'Atalante R/V*. doi: 10.17600/18000884

Guieu, C., Bonnet, S., Petrenko, A., Menkes, C., Chavagnac, V., Desboeufs, K., et al. (2018). Iron from a submarine source impacts the productive layer of the Western Tropical South Pacific (WTSP). *Sci. Rep.* 8, 9075. doi: 10.1038/s41598-018-27407-z

Hassler, C. S., Berg, V. D., and Boyd, P. W. (2017). Toward a regional classification to provide a more inclusive examination of the ocean biogeochemistry of iron-binding ligands. *Front. Mar. Sci.* 4. doi: 10.3389/fmars.2017.00019

Hassler, C. S., Norman, L., Mancuso Nichols, C. A., Clementson, L. A., Robinson, C., Schoemann, V., et al. (2015). Iron associated with exopolymeric substances is highly bioavailable to oceanic phytoplankton. *Mar. Chem. SCOR WG 139: Organic Ligands A Key Control Trace Metal Biogeochem. Ocean* 173, 136–147. doi: 10.1016/j.marchem.2014.10.002

Hassler, C. S., Schoemann, V., Nichols, C. M., Butler, E. C. V., and Boyd, P. W. (2011). Saccharides enhance iron bioavailability to Southern Ocean phytoplankton. *Proc. Natl. Acad. Sci.* 108, 1076–1081. doi: 10.1073/pnas.1010963108

Hawkes, J. A., Connelly, D. P., Gledhill, M., and Achterberg, E. P. (2013). The stabilisation and transportation of dissolved iron from high temperature hydrothermal vent systems. *Earth Planet Sci. Lett.* 375, 280–290. doi: 10.1016/j.epsl.2013.05.047

Heller, M., Gaiero, D., and Croot, P. (2013). Basin scale survey of marine humic fluorescence in the Atlantic: Relationship to iron solubility and H2O2. *Glob. Biogeochem. Cycles* 27 (1), 88–100. doi: 10.1029/2012GB004427

Hioki, N., Kuma, K., Morita, Y., Sasayama, R., Ooki, A., Kondo, Y., et al. (2014). Laterally spreading iron, humic-like dissolved organic matter and nutrients in cold, dense subsurface water of the Arctic Ocean. *Sci. Rep.* 4, 1–9. doi: 10.1038/srep06775

Hoffman, C. L., Monreal, P. J., Albers, J. B., Lough, A. J., Santoro, A. E., Mellett, T., et al. (2023). Microbial strong organic ligand production is tightly coupled to iron in hydrothermal plumes. *bioRxiv*, 2023–01. doi: 10.1101/2023.01.05.522639

Hudson, N., Baker, A., and Reynolds, D. (2007). Fluorescence analysis of dissolved organic matter in natural, waste and polluted waters—a review. *River Res. Appl.* 23, 631–649. doi: 10.1002/rra.1005

Ibisanmi, E., Sander, S. G., Boyd, P. W., Bowie, A. R., and Hunter, K. A. (2011). Vertical distributions of iron-(III) complexing ligands in the Southern Ocean. *Deep Sea Res. Part II: Topical Stud. Oceanography Biogeochem. Aust. Sector South. Ocean* 58, 2113–2125. doi: 10.1016/j.dsr2.2011.05.028

Ishii, S. K. L., and Boyer, T. H. (2012). Behavior of reoccurring PARAFAC components in fluorescent dissolved organic matter in natural and engineered systems: A critical review. *Environ. Sci. Technol.* 46, 2006–2017. doi: 10.1021/es2043504

Jia, K., Manning, C. C. M., Jollymore, A., and Beckie, R. D. (2021). Technical note: Effects of iron(II) on fluorescence properties of dissolved organic matter at circumneutral pH. *Hydrol. Earth Syst. Sci.* 25, 4983–4993. doi: 10.5194/hess-25-4983-2021

Jones, M. E., Beckler, J. S., and Taillefert, M. (2011). The flux of soluble organic-iron (III) complexes from sediments represents a source of stable iron(III) to estuarine waters and to the continental shelf. *Limnol. Oceanogr.* 56, 1811–1823. doi: 10.4319/lo.2011.56.5.1811

Kawabe, M., and Fujio, S. (2010). Pacific ocean circulation based on observation. *J. Oceanogr.* 66, 389–403. doi: 10.1007/s10872-010-0034-8

Kleint, C., Bach, W., Diehl, A., Fröhberg, N., Garbe-Schönberg, D., Hartmann, J. F., et al. (2019). Geochemical characterization of highly diverse hydrothermal fluids from volcanic vent systems of the Kermadec intraoceanic arc. *Chem. Geol.* 528, 119289. doi: 10.1016/j.chemgeo.2019.119289

Kleint, C., Hawkes, J. A., Sander, S. G., and Koschinsky, A. (2016). Voltammetric investigation of hydrothermal iron speciation. *Front. Mar. Sci.* 3. doi: 10.3389/fmars.2016.00075

Kleint, C., Pichler, T., and Koschinsky, A. (2017). Geochemical characteristics, speciation and size-fractionation of iron (Fe) in two marine shallow-water hydrothermal systems, Dominica, Lesser Antilles. *Chem. Geol.* 454, 44–53. doi: 10.1016/j.chemgeo.2017.02.021

Kleint, C., Zitoun, R., Neuholz, R., Walter, M., Schnetger, B., Klose, L., et al. (2022). Trace metal dynamics in shallow hydrothermal plumes at the kermadec arc. *Front. Mar. Sci.* 8. doi: 10.3389/fmars.2021.782734

Klunder, M. B., Laan, P., Middag, R., Baar, H. J. W., and Bakker, K. (2012). Dissolved iron in the Arctic Ocean: Important role of hydrothermal sources, shelf input and scavenging removal. *J. Geophys. Res. Oceans* 117 (C4). doi: 10.1029/2011JC007135

Klunder, M. B., Laan, P., Middag, R., De Baar, H. J. W., and van Ooijen, J. C. (2011). Dissolved iron in the Southern Ocean (Atlantic sector). *Deep Sea Res. Part II Top. Stud. Oceanogr. Physics Carbon Dioxide Trace Elements Isotopes South. Ocean: Polarstern Expeditions ANT XXIV-3 (2008) ANT XXIII/3 (2006)* 58, 2678–2694. doi: 10.1016/j.dsr2.2010.10.042

Komaki, K., and Kawabe, M. (2007). Structure of the upper deep current in the Melanesian Basin, western North Pacific. *Monthly Energy Review* 45, 15–22.

Kondo, Y., Bamba, R., Obata, H., Nishioka, J., and Takeda, S. (2021). Distinct profiles of size-fractionated iron-binding ligands between the eastern and western subarctic Pacific. *Sci. Rep.* 11, 2053. doi: 10.1038/s41598-021-81536-6

Kondo, Y., Takeda, S., and Furuya, K. (2007). Distribution and speciation of dissolved iron in the Sulu Sea and its adjacent waters. *Deep Sea Res. Part II: Topical Stud. Oceanography Biogeochem. Biodiversity Sulu Sea* 54, 60–80. doi: 10.1016/j.dsr2.2006.08.019

Kondo, Y., Takeda, S., and Furuya, K. (2012). Distinct trends in dissolved Fe speciation between shallow and deep waters in the Pacific Ocean. *Mar. Chem.* 134–135, 18–28. doi: 10.1016/j.marchem.2012.03.002

Kraemer, S. M., Butler, A., Borer, P., and Cervini-Silva, J. (2005). Siderophores and the dissolution of iron-bearing minerals in marine systems. *Rev. Mineral. Geochem.* 59, 53–84. doi: 10.2138/rmg.2005.59.4

Laglera, L. M., Battaglia, G., and van den Berg, C. M. G. (2011). Effect of humic substances on the iron speciation in natural waters by CLE/CSV. *Mar. Chem.* 127, 134–143. doi: 10.1016/j.marchem.2011.09.003

Laglera, L. M., Caprara, S., and Monticelli, D. (2016). Towards a zero-blank, preconcentration-free voltammetric method for iron analysis at picomolar concentrations in unbuffered seawater. *Talanta* 150, 449–454. doi: 10.1016/j.talanta.2015.12.060

Laglera, L. M., Sukekava, C., Slagter, H. A., Downes, J., Aparicio-Gonzalez, A., and Gerringa, L. J. A. (2019). First quantification of the controlling role of humic substances in the transport of iron across the surface of the arctic ocean. *Environ. Sci. Technol.* 53, 13136–13145. doi: 10.1021/acs.est.9b04240

Laglera, L. M., and van den Berg, C. M. G. (2009). Evidence for geochemical control of iron by humic substances in seawater. *Limnol. Oceanogr.* 54, 610–619. doi: 10.4319/lo.2009.54.2.0610

Langdon, C. (2010). Determination of Dissolved Oxygen in Seawater by Winkler Titration Using The Amperometric Technique. In, *The GO-SHIP Repeat Hydrography Manual: A Collection of Expert Reports and Guidelines*. Version 1, (eds E. M. Hood, C. L. Sabine and B. M. Sloyan). 18pp. (IOCCP Report Number 14; ICPO Publication Series Number 134). doi: 10.25607/OBP-1350

Lee, Y. P., Wong, K. H., Obata, H., Nishitani, K., Ogawa, H., Fukuda, H., et al. (2023). Distributions of humic substances in an estuarine region (Otsuchi Bay, Japan) determined using electrochemical and optical methods. *Mar. Chem.* 256, 104301. doi: 10.1016/j.marchem.2023.104301

Liu, X., and Millero, F. J. (2002). The solubility of iron in seawater. *Mar. Chem.* 77, 43–54. doi: 10.1016/S0304-4203(01)00074-3

Lory, C., Van Wambeke, F., Fourquez, M., Barani, A., Guieu, C., Tilliette, C., et al. (2022). Assessing the contribution of diazotrophs to microbial Fe uptake using a group specific approach in the Western Tropical South Pacific Ocean. *ISME Commun.* 2, 1–11. doi: 10.1038/s43705-022-00122-7

Mahieu, L. (2023). *Analytical challenges, development and application of CLE-AdCSV for the determination of the organic speciation of iron in marine waters* (University of Liverpool: Doctoral thesis). Available at: https://livrepository.liverpool.ac.uk/3170548/.

Mahieu, L., Omanović, D., Whitby, H., Buck, K. N., Caprara, S., Salaün, P., et al. (2024). Recommendations for best practice for iron speciation by competitive ligand exchange adsorptive cathodic stripping voltammetry with salicylaldoxime. *Mar. Chem.* 104348.

Massoth, G. J., De Ronde, C. E. J., Lupton, J. E., Feely, R. A., Baker, E. T., Lebon, G. T., et al. (2003). Chemically rich and diverse submarine hydrothermal plumes of the southern Kermadec volcanic arc (New Zealand). *Geol. Soc Lond. Spec. Publ.* 219, 119–139. doi: 10.1144/GSL.SP.2003.219.01.06

Mawji, E., Gledhill, M., Milton, J. A., Tarran, G. A., Ussher, S., Thompson, A., et al. (2008). Hydroxamate siderophores: occurrence and importance in the atlantic ocean. *Environ. Sci. Technol.* 42, 8675–8680. doi: 10.1021/es801884r

Ménez, B., Pisapia, C., Andreani, M., Jamme, F., Vanbellingen, Q. P., Brunelle, A., et al. (2018). Abiotic synthesis of amino acids in the recesses of the oceanic lithosphere. *Nature* 564, 59–63. doi: 10.1038/s41586-018-0684-z

Mentges, A., Feenders, C., Seibt, M., Blasius, B., and Dittmar, T. (2017). Functional molecular diversity of marine dissolved organic matter is reduced during degradation. *Front. Mar. Sci.* 4. doi: 10.3389/fmars.2017.00194

Millero, F. J., Sotolongo, S., and Izaguirre, M. (1987). The oxidation kinetics of Fe(II) in seawater. *Geochim. Cosmochim. Acta* 51, 793–801. doi: 10.1016/0016-7037(87)90093-7

Moore, C. M., Mills, M. M., Arrigo, K. R., Berman-Frank, I., Bopp, L., Boyd, P. W., et al. (2013). Processes and patterns of oceanic nutrient limitation. *Nat. Geosci.* 6, 701–710. doi: 10.1038/ngeo1765

Moppert, X., Le Costaouec, T., Raguenes, G., Courtois, A., Simon-Colin, C., Crassous, P., et al. (2009). Investigations into the uptake of copper, iron and selenium by a highly sulphated bacterial exopolysaccharide isolated from microbial mats. *J. Ind. Microbiol. Biotechnol.* 36, 599–604. doi: 10.1007/s10295-009-0529-8

Nelson, N. B., Siegel, D. A., Carlson, C. A., and Swan, C. M. (2010). Tracing global biogeochemical cycles and meridional overturning circulation using chromophoric dissolved organic matter. *Geophys. Res. Lett.* 37. doi: 10.1029/2009GL042325

Nernst, W. (1889). Die elektromotorische Wirksamkeit der Jonen. *Zeitschrift für Physikalische Chemie* 4U, 129–181. doi: 10.1515/zpch-1889-0412

Neuholz, R., Kleint, C., Schnetger, B., Koschinsky, A., Laan, P., Middag, R., et al. (2020). Submarine hydrothermal discharge and fluxes of dissolved fe and mn, and he isotopes at brothers volcano based on radium isotopes. *Minerals* 10, 969. doi: 10.3390/min10110969

Nichols, C. M., Lardière, S. G., Bowman, J. P., Nichols, P. D., Gibson, A. E., and Guézennec, J. (2005). Chemical characterization of exopolysaccharides from Antarctic marine bacteria. *Microb. Ecol.* 49, 578–589. doi: 10.1007/s00248-004-0093-8

Norman, L., Worms, I. A. M., Angles, E., Bowie, A. R., Nichols, C. M., Ninh Pham, A., et al. (2015). The role of bacterial and algal exopolymeric substances in iron chemistry. *Mar. Chem. SCOR WG 139: Organic Ligands A Key Control Trace Metal Biogeochem. Ocean* 173, 148–161. doi: 10.1016/j.marchem.2015.03.015

Ohno, T., Amirbahman, A., and Bro, R. (2008). Parallel factor analysis of excitation–emission matrix fluorescence spectra of water soluble soil organic matter as basis for the determination of conditional metal binding parameters. *Environ. Sci. Technol.* 42, 186–192. doi: 10.1021/es071855f

Omori, Y., Hama, T., Ishii, M., and Saito, S. (2010). Relationship between the seasonal change in fluorescent dissolved organic matter and mixed layer depth in the subtropical western North Pacific. *J. Geophys. Res. Oceans* 115 (C6). doi: 10.1029/2009JC005526

Oudot, C., Gerard, R., Morin, P., and Gningue, I. (1988). Precise shipboard determination of dissolved oxygen (Winkler procedure) for productivity studies with a commercial system1. *Limnol. Oceanogr.* 33, 146–150. doi: 10.4319/lo.1988.33.1.0146

Pernet-Coudrier, B., Waeles, M., Filella, M., Quentel, F., and Riso, R. D. (2013). Simple and simultaneous determination of glutathione, thioacetamide and refractory organic matter in natural waters by DP-CSV. *Sci. Total Environ.* 463–464, 997–1005. doi: 10.1016/j.scitotenv.2013.06.053

Pižeta, I., Sander, S. G., Hudson, R. J. M., Omanović, D., Baars, O., Barbeau, K. A., et al. (2015). Interpretation of complexometric titration data: An intercomparison of methods for estimating models of trace metal complexation by natural organic ligands. *Mar. Chem. SCOR WG 139: Organic Ligands A Key Control Trace Metal Biogeochem. Ocean* 173, 3–24. doi: 10.1016/j.marchem.2015.03.006

Powell, R. T., and Wilson-Finelli, A. (2003). Photochemical degradation of organic iron complexing ligands in seawater. *Aquat. Sci.* 65, 367–374. doi: 10.1007/s00027-003-0679-0

Resing, J. A., Rubin, K. H., Embley, R. W., Lupton, J. E., Baker, E. T., Dziak, R. P., et al. (2011). Active submarine eruption of boninite in the northeastern Lau Basin. *Nat. Geosci.* 4, 799–806. doi: 10.1038/ngeo1275

Resing, J. A., Sedwick, P. N., German, C. R., Jenkins, W. J., Moffett, J. W., Sohst, B. M., et al. (2015). Basin-scale transport of hydrothermal dissolved metals across the South Pacific Ocean. *Nature* 523, 200–203. doi: 10.1038/nature14577

Rickard, D., and Luther, G. W. (2007). Chemistry of iron sulfides. *Chem. Rev.* 107, 514–562. doi: 10.1021/cr0503658

Rijkenberg, M. J. A., Powell, C. F., Dall'Osto, M., Nielsdottir, M. C., Patey, M. D., Hill, P. G., et al. (2008). Changes in iron speciation following a Saharan dust event in the tropical North Atlantic Ocean. *Mar. Chem.* 110, 56–67. doi: 10.1016/j.marchem.2008.02.006

Rougeaux, H., Pichon, R., Kervarec, N., Raguénès, G. H. C., and Guezennec, J. G. (1996). Novel bacterial exopolysaccharides from deep-sea hydrothermal vents. *Carbohydr. Polymers* 31, 237–242. doi: 10.1016/S0144-8617(96)00079-3

Rue, E. L., and Bruland, K. W. (1995). Complexation of iron(III) by natural organic ligands in the Central North Pacific as determined by a new competitive ligand equilibration/adsorptive cathodic stripping voltammetric method. *Mar. Chem. Chem. Iron Seawater Interaction Phytoplankton* 50, 117–138. doi: 10.1016/0304-4203(95)00031-L

Sander, S. G., and Koschinsky, A. (2011). Metal flux from hydrothermal vents increased by organic complexation. *Nat. Geosci.* 4, 145–150. doi: 10.1038/ngeo1088

Santana-Casiano, J. M., González-Santana, D., Devresse, Q., Hepach, H., Santana-González, C., Quack, B., et al. (2022). Exploring the effects of organic matter characteristics on Fe(II) oxidation kinetics in coastal seawater. *Environ. Sci. Technol.* 56, 2718–2728. doi: 10.1021/acs.est.1c04512

Santana-Casiano, J. M., González-Dávila, M., Rodríguez, M. J., and Millero, F. J. (2000). The effect of organic compounds in the oxidation kinetics of Fe(II). *Marine Chemistry* 70, 211–222. doi: 10.1016/s0304-4203(00)00027-x

Sarma, N. S., Kiran, R., Rama Reddy, M., Iyer, S. D., Peketi, A., Borole, D. V., et al. (2018). Hydrothermal alteration promotes humic acid formation in sediments: A case study of the Central Indian Ocean Basin. *J. Geophys. Res. Oceans* 123, 110–130. doi: 10.1002/2017JC012940

Silva, N., Rojas, N., and Fedele, A. (2009). Water masses in the Humboldt Current System: Properties, distribution, and the nitrate deficit as a chemical water mass tracer for Equatorial Subsurface Water off Chile. *Deep Sea Res. Part II Top. Stud. Oceanogr. Oceanography Eastern South Pacific II: Oxygen Minimum Zone* 56, 1004–1020. doi: 10.1016/j.dsr2.2008.12.013

Slagter, H. A., Reader, H. E., Rijkenberg, M. J. A., van der Loeff, M. R., De Baar, H. J. W., and Gerringa, L. J. A. (2017). Organic Fe speciation in the Eurasian Basins of the Arctic Ocean and its relation to terrestrial DOM. *Mar. Chem.* 197, 11–25. doi: 10.1016/j.marchem.2017.10.005

Sohrin, R., and Sempéré, R. (2005). Seasonal variation in total organic carbon in the northeast Atlantic in 2000–2001. *J. Geophys. Res. Oceans* 110 (C10). doi: 10.1029/2004JC002731

Spearman, C. (1904). The proof and measurement of association between two things. *Am. J. Psychol.* 15, 72–101. doi: 10.2307/1412159

Stedmon, C., and Álvarez-Salgado, X. A. (2011). Shedding light on a black box: UV–Visible spectroscopic characterization of marine dissolved organic matter. *American Association for the Advancement of Science*. doi: 10.1126/science.opms.sb0001

Sukekava, C. F., Andrade, C. F. F., Niencheski, L. F. H., de Souza, M. S., and Laglera, L. M. (2023). Macronutrients, iron and humic substances summer cycling over the extended continental shelf of the South Brazil Bight. *Sci. Total Environ.* 865, 161182. doi: 10.1016/j.scitotenv.2022.161182

Sukekava, C. F., Downes, J., Filella, M., Vilanova, B., and Laglera, L. (2024). Ligand exchange provides new insight into the role of humic substances in the marine iron cycle. *Geochim. Cosmochim. Acta* 366, 17–30. doi: 10.1016/j.gca.2023.12.007

Sukekava, C., Downes, J., Slagter, H. A., Gerringa, L. J. A., and Laglera, L. M. (2018). Determination of the contribution of humic substances to iron complexation in seawater by catalytic cathodic stripping voltammetry. *Talanta* 189, 359–364. doi: 10.1016/j.talanta.2018.07.021

Summers, N., and Watling, L. (2021). Upper Bathyal Pacific Ocean biogeographic provinces from octocoral distributions. *Prog. Oceanogr.* 191, 102509. doi: 10.1016/j.pocean.2020.102509

Tagliabue, A., Buck, K. N., Sofen, L. E., Twining, B. S., Aumont, O., Boyd, P. W., et al. (2023). Authigenic mineral phases as a driver of the upper-ocean iron cycle. *Nature* 620, 104–109. doi: 10.1038/s41586-023-06210-5

Tagliabue, A., Mtshali, T., Aumont, O., Bowie, A. R., Klunder, M. B., Roychoudhury, A. N., et al. (2012). A global compilation of dissolved iron measurements: focus on distributions and processes in the Southern Ocean. *Biogeosciences* 9 (6), 2333–2349. doi: 10.5194/bg-9-2333-2012

Tagliabue, A., and Resing, J. (2016). Impact of hydrothermalism on the ocean iron cycle. *Philos. Trans. R. Soc. A: Mathematical Phys. Eng. Sci.* 374, 20150291. doi: 10.1098/rsta.2015.0291

Talley, L. D., Pickard, G. L., Emery, W. J., and Swift, J. H. (2011). Chapter 10 - Pacific Ocean. *Descriptive Physical Oceanography* (*Sixth* Edition) Eds. L. D. Talley, G. L. Pickard, W. J. Emery and J. H. Swift. (Boston: Academic Press), 303–362. doi: 10.1016/B978-0-7506-4552-2.10010-1

Tani, H., Nishioka, J., Kuma, K., Takata, H., Yamashita, Y., Tanoue, E., et al. (2003). Iron(III) hydroxide solubility and humic-type fluorescent organic matter in the deep water column of the Okhotsk Sea and the northwestern North Pacific Ocean. *Deep Sea Res. Part Oceanogr. Res. Pap.* 50, 1063–1078. doi: 10.1016/S0967-0637(03)00098-0

Tedetti, M., Bigot, L., Turquet, J., Guigue, C., Ferretto, N., Goutx, M., et al. (2020). Influence of freshwater discharges on biogeochemistry and benthic communities of a coral reef ecosystem (La Réunion Island, Indian Ocean). *Front. Mar. Sci.* 7. doi: 10.3389/fmars.2020.596165

Tilliette, C., Gazeau, F., Portlock, G., Benavides, M., Bonnet, S., Guigue, C., et al. (2023). Influence of shallow hydrothermal fluid release on the functioning of phytoplankton communities. *Front. Mar. Sci.* 10. doi: 10.3389/fmars.2023.1082077

Tilliette, C., Taillandier, V., Bouruet-Aubertot, P., Grima, N., Maes, C., Montanes, M., et al. (2022). Dissolved iron patterns impacted by shallow hydrothermal sources along a transect through the Tonga-kermadec arc. *Glob. Biogeochem. Cycles* 36, e2022GB007363. doi: 10.1029/2022GB007363

Timm, C., Bassett, D., Graham, I. J., Leybourne, M. I., de Ronde, C. E. J., Woodhead, J., et al. (2013). Louisville seamount subduction and its implication on mantle flow beneath the central Tonga–Kermadec arc. *Nat Commun* 4, 1720. doi: 10.1038/ncomms2702

Thuróczy, C.-E., Gerringa, L. J. A., Klunder, M., Laan, P., Le Guitton, M., de Baar, H. J. W., et al. (2011). Distinct trends in the speciation of iron between the shallow shelf seas and the deep basins of the Arctic Ocean. *J. Geophys. Res.* 116. doi: 10.1029/2010JC006835

Toner, B. M., Fakra, S. C., Manganini, S. J., Santelli, C. M., Marcus, M. A., Moffett, J. W., et al. (2009). Preservation of iron(II) by carbon-rich matrices in a hydrothermal plume. *Nat. Geosci.* 2, 197–201. doi: 10.1038/ngeo433

Tonnard, M., Planquette, H., Bowie, A. R., van der Merwe, P., Gallinari, M., Desprez de Gésincourt, F., et al. (2020). Dissolved iron in the North Atlantic Ocean and Labrador Sea along the GEOVIDE section (GEOTRACES section GA01). *Biogeosciences* 17, 917–943. doi: 10.5194/bg-17-917-2020

Town, R. M., and Filella, M. (2000). Dispelling the myths: Is the existence of L1 and L2 ligands necessary to explain metal ion speciation in natural waters? *Limnol. Oceanogr.* 45, 1341–1357. doi: 10.4319/lo.2000.45.6.1341

Twining, B. S., and Baines, S. B. (2013). The trace metal composition of marine phytoplankton. *Annu. Rev. Mar. Sci.* 5, 191–215. doi: 10.1146/annurev-marine-121211-172322

van den Berg, C. M. G. (1995). Evidence for organic complexation of iron in seawater. *Mar. Chem. Chem. Iron Seawater Interaction Phytoplankton* 50, 139–157. doi: 10.1016/0304-4203(95)00032-M

van den Berg, C. M. G. (2006). Chemical speciation of iron in seawater by cathodic stripping voltammetry with dihydroxynaphthalene. *Anal. Chem.* 78, 156–163. doi: 10.1021/ac051441

Velasquez, I. B., Ibisanmi, E., Maas, E. W., Boyd, P. W., Nodder, S., and Sander, S. G. (2016). Ferrioxamine Siderophores Detected amongst Iron Binding Ligands Produced during the Remineralization of Marine Particles. *Front. Mar. Sci.* 3. doi: 10.3389/fmars.2016.00172

Wang, H., Resing, J. A., Yan, Q., Buck, N. J., Michael, S. M., Zhou, H., et al. (2021). The characteristics of Fe speciation and Fe-binding ligands in the Mariana back-arc hydrothermal plumes. *Geochim. Cosmochim. Acta* 292, 24–36. doi: 10.1016/j.gca.2020.09.016

Wang, H., Wang, W., Liu, M., Zhou, H., Ellwood, M. J., Butterfield, D. A., et al. (2022). Iron ligands and isotopes in hydrothermal plumes over backarc volcanoes in the Northeast Lau Basin, Southwest Pacific Ocean. *Geochim. Cosmochim. Acta* 336, 341–352. doi: 10.1016/j.gca.2022.09.026

Whitby, H., Bressac, M., Sarthou, G., Ellwood, M. J., Guieu, C., and Boyd, P. W. (2020a). Contribution of electroactive humic substances to the iron-binding ligands released during microbial remineralization of sinking particles. *Geophys. Res. Lett.* 47, e2019GL086685. doi: 10.1029/2019GL086685

Whitby, H., Planquette, H., Cassar, N., Bucciarelli, E., Osburn, C. L., Janssen, D. J., et al. (2020b). A call for refining the role of humic-like substances in the oceanic iron cycle. *Sci. Rep.* 10, 1–12. doi: 10.1038/s41598-020-62266-7

Whitby, H., and van den Berg, C. M. G. (2015). Evidence for copper-binding humic substances in seawater. *Mar. Chem. SCOR WG 139: Organic Ligands A Key Control Trace Metal Biogeochem. Ocean* 173, 282–290. doi: 10.1016/j.marchem.2014.09.011

Winkler, L. W. (1888). Die Bestimmung des im Wasser gelösten Sauerstoffes. Berichte der deutschen chemischen. *Gesellschaft* 21, 2843–2854. doi: 10.1002/cber.188802102122

Witter, A. E., and Luther, G. W. (1998). Variation in Fe-organic complexation with depth in the Northwestern Atlantic Ocean as determined using a kinetic approach. *Mar. Chem.* 62, 241–258. doi: 10.1016/S0304-4203(98)00044-9

Yamashita, Y., Hashihama, F., Saito, H., Fukuda, H., and Ogawa, H. (2017). Factors controlling the geographical distribution of fluorescent dissolved organic matter in the surface waters of the Pacific Ocean. *Limnol. Oceanogr.* 62, 2360–2374. doi: 10.1002/lno.10570

Yang, L., Hong, H., Guo, W., Chen, C.-T. A., Pan, P.-I., and Feng, C.-C. (2012). Absorption and fluorescence of dissolved organic matter in submarine hydrothermal vents off NE Taiwan. *Mar. Chem.* 128–129, 64–71. doi: 10.1016/j.marchem.2011.10.003

Yang, R., and van den Berg, C. M. G. (2009). Metal complexation by humic substances in seawater. *Environ. Sci. Technol.* 43, 7192–7197. doi: 10.1021/es900173w

Yücel, M., Gartman, A., Chan, C. S., and Luther, G. W. (2011). Hydrothermal vents as a kinetically stable source of iron-sulphide-bearing nanoparticles to the ocean. *Nat. Geosci.* 4, 367–371. doi: 10.1038/ngeo1148

Yücel, M., Sevgen, S., and Le Bris, N. (2021). Soluble, colloidal, and particulate iron across the hydrothermal vent mixing zones in broken spur and rainbow, mid-atlantic ridge. *Front. Microbiol.* 12. doi: 10.3389/fmicb.2021.631885

Zhao, J., and Nelson, D. J. (2005). Fluorescence study of the interaction of Suwannee River fulvic acid with metal ions and Al3+-metal ion competition. *J. Inorganic Biochem.* 99, 383–396. doi: 10.1016/j.jinorgbio.2004.10.005

Zigah, P. K., McNichol, A. P., Xu, L., Johnson, C., Santinelli, C., Karl, D. M., et al. (2017). Allochthonous sources and dynamic cycling of ocean dissolved organic carbon revealed by carbon isotopes. *Geophys. Res. Lett.* 44, 2407–2415. doi: 10.1002/2016GL071348